A Mathematical Model for the Maneuvering Simulation of a Propelled SPAR Vessel

By

©Soroosh Mohammadafzali

A thesis submitted to the

School of Graduate Studies

in partial fulfillment of the requirements for the degree of

MASTER OF ENGINEERING

Faculty of Engineering and Applied Science

Memorial University of Newfoundland

St. John's Newfoundland and Labrador

Abstract

To predict the maneuvering performance of a propelled SPAR vessel, a mathematical model was established as a path simulator. A system-based mathematical model was chosen as it offers advantages in cost and time over full Computational Fluid Dynamics (CFD) simulations. The model is intended to provide a means of optimizing the maneuvering performance of this new vessel type.

In this study the hydrodynamic forces and control forces are investigated as individual components, combined in a vectorial setting, and transferred to a body-fixed basis. SPAR vessels are known to be very sensitive to large amplitude motions during maneuvers due to the relatively small hydrostatic restoring forces. Previous model tests of SPAR vessels have shown significant roll and pitch amplitudes, especially during course change maneuvers. Thus, a full 6 DOF equation of motion was employed in the current numerical model.

The mathematical model employed in this study was a combination of the model introduced by the Maneuvering Modeling Group (MMG) and the Abkowitz (1964) model. The new model represents the forces applied to the ship hull, the propeller forces and the rudder forces independently, as proposed by the MMG, but uses a 6DOF equation of motion introduced by Abkowitz to describe the motion of a maneuvering ship.

The mathematical model was used to simulate the trajectory and motions of the propelled SPAR vessel in 10˚/10˚, 20˚/20˚ and 30˚/30˚ standard zig-zag maneuvers, as well as

turning circle tests at rudder angles of 20˚ and 30˚. The simulation results were used to determine the maneuverability parameters (e.g. advance, transfer and tactical diameter) of the vessel. The final model provides the means of predicting and assessing the performance of the vessel type and can be easily adapted to specific vessel configurations based on the generic SPAR-type vessel used in this study.

Acknowledgments

I would like to express my sincere thanks and gratitude to my supervisors Dr. Brian Veitch and Dr. Bruce Colbourne for their unsparing support, guidance, advice and financial support through the course of this work. They will remain as the perfect example of kind and professional supervisors in my mind.

I would also like to thank Andrew MacNeill who offered me his generous help and shared his valuable experience with me during my experiments. Without him, completion of this project could not have been accomplished. To Pearl Li, Rafael Cotrim Ferreira Oliveira Botelho and Trevor Clark, I appreciate the time and assistance you offered me to accomplish this project.

Finally, to my encouraging, caring and loving wife: Ladan, my deepest gratitude. You are the one who held my hand during all the steps, helped me when I asked for help, relieved me when I was disturbed and stayed awake for me to return home. Thank you.

Table of contents

List of tables

List of figures

List of symbols

∇_0	Volume of displacement
A_R	Profile area of movable part of mariner rudder
A_{WP}	Water plane area
D_P	Propeller diameter
i, j, k	Unit vectors associated with x, y, z
I, J, K	Unit vectors associated with x_0, y_0, z_0
J_P	Propeller advance ratio
K, M, N	External moments with respect to roll, pitch and yaw
K_T	Thrust coefficient
n_P	Propeller revolution
$o\_ x, y, z$	Body fixed coordinate system originated at center of gravity

$o_0 \_ x_0, y_0, z_0$	Space fixed coordinate system
p, q, r	Roll, pitch and yaw rates
r'	Non-dimensionalized yaw rate
R_0	Position of the ship's origin
Subscripts *R, HS, P, A, G-B*	Rudder forces, steady hydrodynamic forces, propulsion, added mass and gravity buoyancy forces
S_x, S_{xx}, S_{yy}	Water plane moments
T	Propeller trust
t_P	Trust deduction factor
U_R	Resultant inflow velocity to the rudder
V_A	Speed of advance
X, Y, Z	External forces with respect to surge, sway and heave

X'_R, Y'_R, K'_R, N'_R	Non-dimensional hydrodynamic coefficients of rudder for maneuvering
z_G, z_B	Height of CoG and height of center of buoyancy
α	Heading angle
β	Drift angle
ϕ, θ, ψ	Roll, pitch and yaw angles
U_0	Velocity of the origin
α_R	Effective inflow angle to the rudder
λ	Scaling factor

1 Introduction

1.1 Background and motivation

The operational function of marine vessels in higher sea conditions has always been a challenge for the marine industry. The concentration of hydrodynamic forces at the sea surface, i.e. wave and flow forces, in harsh sea states cause severe motions that impair the vessel's service.

The propelled SPAR vessel which was developed at MUN and has been commercialized under the name TranSPAR attempts to address this problem and has been under development since 2010, when it was selected as one of the top projects in the Carbon Trust's, Offshore Wind Accelerator (OWA) Access competition. The SPAR-type vessel is a unique solution to the problem of reduced vessel motions. Based on a combination of offshore structure technology with a vessel concept, the propelled SPAR was originally designed as a service vessel to transfer personnel and equipment to offshore wind turbines. However, this type of vessel could be applicable in a wide range of the ocean industries where small, stable vessels are required.

The SPAR-type vessel concept is under continuing development and there are areas where the performance of vessels with surface piercing struts might be improved through better understanding of the performance parameters and the links between the physical characteristics and the dynamic response of the vessel. The significant feature of the vessel type is the relatively small strut that links the submerged body of the vessel to the

above water load-carrying cab of the vessel. Although this feature directly addresses the reduction of wave-induced motions, the slenderness of the strut introduces challenges in terms of the controllability and maneuverability of the vessel.

Figure 1- The Tran-SPAR vessel model

In this research, the maneuvering performance of the propelled-SPAR vessel will be examined through numerical simulation. Moreover, this research will study the characteristics of the SPAR-type vessel to better understand the influence of the main vessel characteristics such as the weight distribution of the struts and the immersed propeller hull and the position of the rudder and thruster, in maneuvering performance of the vessel. Better understanding of these aspects of the vessel performance may lead to

overall improvements in the performance of SPAR type vessels or other applications where specialized vessels or vehicles make use of surface piercing struts.

This research is based on a combination of numerical models and physical model tests to understand and optimize vessel performance. The mathematical analysis is based on physical laws governing bodies in fluids and boundary conditions. A numerical computing environment was employed to solve the governing equations in a real-time simulation.

1.2 Scope of work

To predict the vessel trajectory under certain controlled circumstances and simulate its motions, the equation of motion is expressed and solved at each time-step of a real-time simulation. The equation of motion for the maneuvering motion of ships is normally expressed in 3 or 4 degrees of freedom (DOF) as the roll, pitch and heave motions are relatively small and their effect in the maneuvering of the ship is negligible. However, for the case of this study, as the roll, pitch and heave motions are significant due to the long surface piercing strut, the equation of motion is expressed in 6 DOF, which describe all axial and rotational motions of the vessel.

In order to solve the equation of motion at each time step, the forces and moments on the vessel are expressed as rudder forces, steady hydrodynamic forces, propulsion, added mass, gravity and buoyancy forces. In this study, rudder forces and steady hydrodynamic forces are measured experimentally and then mathematically modeled. Propulsion and restoring forces are estimated by empirical formulations based on the geometry of the

vessel, and added mass coefficients are obtained by the boundary integral equation method.

MATLAB software is employed to complete the real-time numerical simulation of the vessel maneuvering. In this phase, a comprehensive model of the dynamic behavior of the vessel is achieved.

The numerical model is used to simulate the trajectory and motions of the propelled SPAR in 10˚/10˚ , 20˚/20˚ and 30˚/30˚ standard zig-zag maneuvers, as well as turning circle tests at rudder angles of 20˚ and 30˚. The simulation results are used to determine maneuverability parameters (e.g. advance, transfer and tactical diameter) of the vessel.

The final model provides the means of predicting and assessing the performance of the SPAR vessel and can be easily adapted to specific vessel configurations based on the generic SPAR-type vessel used in this study. In this study, some geometrical characteristics of the vessel such as the weight distribution of struts and immersed propeller hull (affecting the center of gravity), and the position of the rudder and thruster are modified to observe their influence in the maneuvering performance of the vessel type and suggest an enhanced geometry in terms of maneuverability.

1.3 Outline of the thesis

This thesis is presented in 6 chapters:

1.3.1 Chapter 1 – Introduction

The first chapter introduces the purpose and outline of the study.

1.3.2 Chapter 2 – Literature review

In this chapter experimental and analytical methods to study the maneuvering performance of a marine vessel are introduced and compared. Predictions based on captive model tests and simulations are represented in more detail as this method is the basic idea behind this study.

1.3.3 Chapter 3 – Mathematical model of the maneuvering

In chapter 3 the coordinate systems that the mathematical model is based on are introduced. The equation of motion is then expressed based on the body-fixed coordinate system. The forces and moments acting on the vessel are then expressed as rudder forces, steady hydrodynamic forces, propulsion, added mass, gravity and buoyancy forces. The procedure for evaluating forces and moments is also described in this chapter.

1.3.4 Chapter 4 – Experimental procedure

In this chapter, the procedure of the experiments is explained. In the first part, the instruments used in the experiments are introduced and the calibration procedure and results are shown. 75 model towing experiments in various yaw angles, rudder angles and towing speeds were conducted and the results are presented in this chapter.

1.3.5 Chapter 5 – Results and discussion

The mathematical model introduced in chapter 3 is used to simulate the vessel trajectory and motions during standard zig-zag and turning circle maneuvers. The outcomes of the

simulations, along with maneuvering characteristics of the vessel determined from the simulations, are presented in this chapter.

1.3.6 Chapter 6 – Conclusions and recommendations

In this chapter the assumption made in the study, concluding remarks and recommendations for a future study are presented.

2 Literature Review

In this section, the state-of-the-art methods used to predict the maneuvering of a marine vessel are introduced and discussed. The purpose of this review is to find the most accurate, responsive, fast and flexible simulation method applicable for the case of this study under limitations of time and instrumentation.

To predict the maneuvering parameters of a ship, the forces and moments acting on ship must be determined. These forces and moments are then used to complete the equation of motion. According to Kim et al.(2008), the amount of computational resources available to predict the maneuvering of a vessel changes year-to-year due to advances in technology. In the following, the methods used to determine hydrodynamic forces on the ships are summarized and compared.

2.1 Mathematical models to predict ship maneuvering

There are several mathematical models to describe the forces and moments acting on a ship, including Abkowitz (1964) polynomial model, Blanke's (1998) 2^{nd} order modulus expansion model, the model based on “principles of low aspect-ratio aerodynamic theory and Lagrangian mechanics” introduced by Ross (2007), and the model developed by the Maneuvering Mathematical Modeling Group (MMG) in Japan, which studies the forces on ship components individually (Araki et al. 2012). Among these models, the Abkowitz model and the MMG model are the most accepted and widely-used models.

The equation of motion at the center of gravity for a maneuvering ship with 3 degrees of freedom is expressed as (Zaojian 2006):

$$X = m(\dot{u} - vr)$$

$$Y = m(\dot{v} + ur) \qquad (1)$$

$$N = I_z\dot{r}$$

where X, Y and N are the external forces and moments acting on the ship, m denotes the total mass, u and v denote surge and sway velocity and r denotes the yaw rate.

In the Abkowitz model, the hydrodynamic forces on the ship are expressed as a polynomial function of maneuvering parameters and control parameters, i.e. the propeller revolution and rudder angle, in form of the Taylor's series. In this model, by partial differentiation of hydrodynamic forces with respect to each variable, the hydrodynamic derivatives can be obtained (Yoon & Rhee 2003). Zaojian (2006) expresses the hydrodynamic forces and moments on the Abkowitz model as:

$$X = X(u, v, r, \dot{u}, \dot{v}, \dot{r}, \delta)$$

$$Y = Y(u, v, r, \dot{u}, \dot{v}, \dot{r}, \delta) \qquad (2)$$

$$N = N(u, v, r, \dot{u}, \dot{v}, \dot{r}, \delta)$$

where δ denotes the rudder angle.

In the MMG model, the hydrodynamic forces acting on a ship are studied individually for the hull, propeller and rudder. Taking the interaction between these forces into account is

critical in the MMG model (Yoon & Rhee 2003). The hydrodynamic forces and moments in this model are expressed as (Zaojian 2006):

$$X = X_H + X_P + X_R$$

$$Y = Y_H + Y_P + Y_R \qquad (3)$$

$$N = N_H + N_P + N_R$$

The main difference between the Abkowitz model and the MMG model is the method they use to obtain the hydrodynamic forces acting on a maneuvering ship. The Abkowitz model studies all the hydrodynamic forces simultaneously, whereas the MMG model breaks the hydrodynamic forces into hull, propeller, rudder forces, and their interactions. The state of the art methods used to evaluate these forces are described in detail in the next section.

In reality, the hydrodynamic forces are composed of steady and non-steady contributions, which make it very difficult to build a descriptive mathematical model. Hence, the hydrodynamic forces on a ship are assumed to be a function of the velocity and acceleration components only. This assumption is known as the "quasi-steady approach" (Yoshimura 2005).

2.2 Methods for determining the hydrodynamic forces acting on a maneuvering ship

The hydrodynamic derivatives in the equation of motion must be determined in order to solve this equation in the time domain and perform a simulation. Accurately determining

these coefficients is sometimes hard to achieve due to the non-linearity of the ship's maneuvering (Luo et al. 2014). Zaojian (2006) effectively categorizes the methods to determine forces and moments acting on a ship in four categories:

2.2.1 Captive model tests

Captive model tests have proved to be the most accurate way to determine the hydrodynamic force coefficients of the ship. However, due to the high cost of conducting these tests and the limited availability of the experimental facilities, sometimes institutions and companies cannot use this method, or must limit the number of experiments (Luo et al. 2014).

Captive model tests are usually conducted in a long and narrow towing tank. A seakeeping and maneuvering basin is sometimes employed to carry out a Circular Motion Test (CMT) (Zaojian 2006). The hydrodynamic derivatives of a ship are obtained by three types of captive model tests (ITTC 2002a):

2.2.1.1 Oblique/straight towing test in a conventional towing tank

In the stationary oblique/straight towing test, the drift angle of the vessel is fixed during each experiment. Maneuvering parameters such as rudder angle, propeller revolution, drift angle and towing velocity might be changed during experiments to determine the hydrodynamic forces as a function of these parameters. Four types of towing tests can be carried out with this method (ITTC 2002a):

Straight towing;

Straight towing with rudder deflection;

Oblique towing;

Oblique towing with rudder deflection.

2.2.1.2 Planar motion test in a tank equipped with a Planar Motion Mechanism (PMM)

A PMM system consists of electromechanical equipment which is designed to tow a vessel model in a pre-programed path in a towing tank. Forces and moments on the model are measured during this procedure and are used to predict the maneuvering performance of the full-scale vessel (Millan & Thorburn 2009). This device is widely used to carry out four types of tests (ITTC 2002a):

Pure sway;

Pure yaw;

Pure yaw with rudder deflection;

Pure yaw with drift.

2.2.1.3 Circular tests in a tank equipped with a rotating arm carriage

Like the oblique/straight towing facility and PMM facility, the Rotating Arm Facility (RAF) is also designed to perform captive towing experiments to measure forces and moments on a model vessel. As the name of this facility indicates, it is designed to tow the vessel in circular orbits across water by means of a rotating arm (Orfano 2009). Four types of circular towing tests are widely conducted in this facility (ITTC 2002a):

Pure yaw;

Yaw with drift;

Yaw with rudder deflection;

Yaw with drift and rudder deflection.

Among the tests mentioned above, the ones with no rudder deflection are carried out to determine the forces on the hull. Tests with rudder deflection are designed to measure rudder induced forces and therefore they are not applicable to models with no rudder and propeller installed.

2.2.2 System identification technique

Another method to determine the hydrodynamic derivatives of a vessel is to conduct a free-running model or full-scale test. In this method, the control parameters, such as the rudder angle and the propeller revolution, are input data and the kinematic reaction to these inputs, such as the velocity and the acceleration, are output data. Hydrodynamic derivatives of the vessel are determined using parameter identification methods (Zaojian 2006).

The traditional methods to identify the maneuvering derivatives of a ship such as the least square method and extended Kalman filter are widely used. Estimation Before Modeling (EBM), also called the two-step method, is an important system identification method to determine the maneuvering coefficients. In this method the hydrodynamic coefficients can be estimated by means of the extended Kalman filter and modified Bryson–Frazier smoother from sea trials (Yoon & Rhee 2003). However, using these methods might affect the accuracy of the prediction since the estimations depend on the target of study and initial guess. Artificial Neural Networks (ANN) can significantly overcome these

limitations and provide an effective means of determining maneuvering derivatives. This method has been used to identify the ship maneuvering derivatives. For example, Zhang and Zou (2011) used the data of a 10˚/10˚ zig-zag test to identify the derivatives in the Abkowitz model and predicted the maneuvering of the same ship in 20˚/20˚ maneuvering. The results show a very good consistency between predicted and simulated results.

2.2.3 Semi-empirical methods (database methods)

The third method to estimate the hydrodynamic derivatives of a vessel is to gather a database of hydrodynamic derivatives of similar vessels. These values can be empirically formulated and used to determine the hydrodynamic derivatives of any of the same type of vessel (Zaojian 2006). However, this method is not always accurate and reliable, especially when the specifications of the studied object are not consistent with the database (Luo et al. 2014) .

2.2.4 Numerical methods

Computational Fluid Dynamics (CFD) is being widely used to determine the forces and moments on a moving vessel. CFD methods can be generally classified into two categories:

1. Potential flow theory methods (e.g. Boundary Element Method (BEM) or panel method)

2. Predictions based on viscous flow theory (e.g. solution of Reynolds-Averaged Navier-Stokes (RANS) equations) (Zaojian 2006).

2.2.5 Comparison

Running a sufficient number of simulations using CFD is a very time and money consuming approach, but it requires only the ship geometry along with propulsion system characteristics to predict the maneuvering of the ship. On the other hand, system-based methods are more accurate and faster to determine the maneuvering derivative, but they also need access to the test facilities and numerous captive model tests need to be conducted to estimate the maneuvering coefficients (Araki et al. 2012).

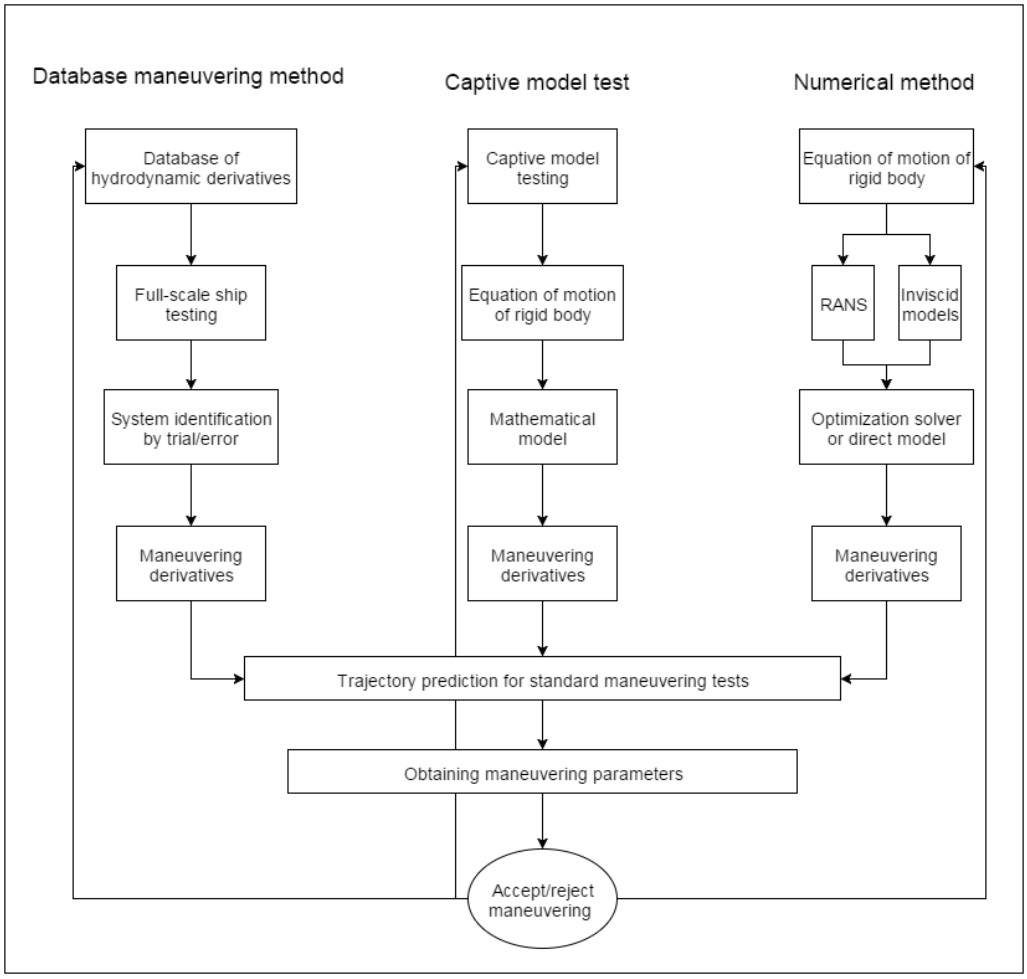

Figure 2- Overview of maneuvering prediction methods (Tran Khanh et al. 2013)

Maimun et al. (2011) indicates that obtaining the hydrodynamic coefficients by means of captive model tests generates more accurate results in comparison with empirical formulations. Comparison between empirical methods and CFD based methods indicates that predictions using both the viscous flow calculations and the slender-body coefficients method are closer than empirical formulas to the experimental results (Toxopeus 2009).

2.3 Control application

Understanding the dynamic characteristics of the ship is the key to designing the control system. It is understood that predicting the maneuvering characteristics of a vessel from model tests is hard due to the lack of knowledge of the interaction between rudder deflection and roll motion. This is especially true for the case of this study. Thus, identifying and analyzing these interactions are essential not only to obtain a comprehensive maneuvering model, but also to design a proper control system (Perez & Blanke 2002).

Identifying the maneuvering derivatives of a ship also allows path simulation in the time domain with respect to the control settings. One of the main applications of these simulations is for training simulators. To be as realistic as possible, the training simulators generally use the full equation of motion (Yoon & Rhee 2003).

2.4 Purpose of study and methodology

The purpose of this research is to develop a mathematical model of maneuvering for a propelled SPAR vessel with the following properties:

- The model must be able to simulate the maneuvering motion of a propelled SPAR vessel in the standard maneuvering tests, such as the zig-zag test and the turning circle test.
- The dynamic and kinematic parameters of the ship, such as roll angle, drift angle, lateral force and moment, velocities, etc. must be measurable at any given time during the simulation to provide the means of better understanding of dynamic behavior of the vessel type.
- The mathematical model, should be adjustable in terms of the vessel geometry, since one of the main purposes of this study is to find effective ways to improve the maneuvering performance of the vessel type by changing the main dimensions.
- The simulation time should be minimized to enable the user to study the maneuvering performance of the vessel in various test types, vessel sizes and new configurations.

To achieve these goals and due to limitations of time and resources, the best achievable method in each step is taken as follows:

2.4.1 Method selection to determine the hydrodynamic forces acting on the maneuvering ship

The CFD simulations are time consuming; simulating the maneuvering of the ships with this method might take few days to few weeks depending on the experiment conditions

and mesh sizes. Hence, for this study as numerous maneuvering tests for the few ship geometries are to be conducted, this method is not applicable.

To determine the forces on the ship using semi-empirical methods, a database consisting of the test results for many same type vessels is needed. As the object of this research is not a conventional vessel, there is no database available to extract the hydrodynamic derivatives.

To obtain the hydrodynamic derivatives of a ship using the system identification method, the ship model needs to be equipped with an accurate control system and motion tracking systems. Due to the small size of the available model and the inaccuracy of the installed control system, precise application and monitoring of the controls is not achievable. Moreover, the small size of the ship results in significant effect of the currents on the performance of the vessel.

According to the above mentioned conditions and limitations, the best and only achievable method to determine the forces on the ship for this study is the captive model test. Furthermore, as mentioned earlier, this method is the most accurate and reliable method at the moment to determine the hydrodynamic coefficients of the ship.

2.4.2 Captive model test mechanism selection

Among the mechanisms to conduct captive model tests, the PMM and RAF tests obtain the most accurate hydrodynamic model for the ship, as they are able to define the hydrodynamic forces as a function of both magnitude and rate of motion parameters such as the yaw angle. However, the available towing tank at MUN is not equipped with the

PMM and RAF systems. Moreover, as the vessel is at the design stage and is not commercialized, the high cost of conducting these types of tests is not reasonable at this time. Thus, in this study the stationary oblique/straight towing tests are selected as the captive model test method. This type of captive model tests are widely used by many researchers, and it is proven that, if conducted properly, they can result in reliable outcomes.

2.4.3 Mathematical model

The mathematical model employed in this study, is a combination of MMG model and the Abkowitz (1964) model. This model represents the forces applied to the ship's hull, the propeller and the rudder, and the interactions between these forces independently, as proposed by the MMG, but uses a 6DOF equation of motion introduced by Abkowitz to describe the motion of a maneuvering ship.

3 Mathematical model of maneuvering

In this chapter the development of the mathematical model used to simulate the trajectory of the propelled SPAR vessel is introduced and forces and moments acting on the vessel are evaluated.

3.1 Equation of motion at center of gravity

In order to describe forces acting on the vessel and the resulting maneuvering motions of the vessel, two coordinate systems were employed: the body-fixed coordinate system that has its origin at the center of gravity and moves with the ship, and an earth-fixed coordinate system that lies on the calm water surface.

Figure 2 demonstrates the two coordinate systems used in this study. The origin *o* of the body-fixed coordinate system is located at the center of gravity and axes *x, y* and *z* lie on the ship's bow, ship's starboard and perpendicular to the *xy* plane downward, respectively. The origin of the earth-fixed coordinate system o_0 is fixed on the calm water surface and is aligned with the initial position of the body-fixed system, the x_0y_0 plane coincides with the calm water surface and the z_0 axis is vertical downward.

Unit vectors associated with *x, y, z,* x_0, y_0 and z_0 are denoted as *i, j, k, I, J* and *K* respectively. Vector R_0 can be defined as the position of the ship's origin (CoG):

$$R_0 = \xi_0 I + \eta_0 J + \zeta_0 K \qquad (4)$$

So the velocity of the origin is expressed as:

$$U_0 = \frac{dR_0}{dt} \qquad (5)$$

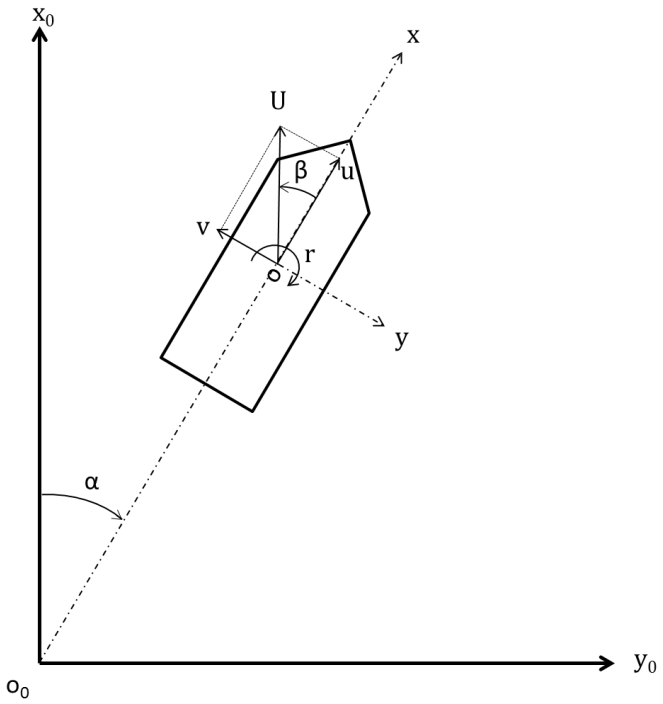

Figure 3- Coordinate systems

u and v are the surge velocity and lateral velocity at the center of gravity, p, q and r are roll, pitch and yaw angles, β and α denote the drift angle of the origin and heading angle respectively.

For a small perturbation, it can be shown that:

$$x_{t+\varepsilon} = x_t + u_t \cos \alpha_t + v_t \sin \alpha_t$$

$$y_{t+\varepsilon} = y_t + u_t \sin \alpha_t - v_t \cos \alpha_t$$

$$z_{t+\varepsilon} = z_t + w_t t$$

$$\phi_{t+\varepsilon} = \phi_t + p_t t$$

$$\theta_{t+\varepsilon} = \theta_t + q_t t$$

$$\psi_{t+\varepsilon} = \psi_t + r_t t \qquad (6)$$

Where the subscript t denotes the value of a parameter at time t and ε represents a small increment in time. ϕ, θ and ψ are roll, pitch and yaw angles respectively.

In this study, the body-fixed coordinate system is used to express the equation of motion and evaluate the hydrodynamic forces. Assuming the vessel is a rigid body with six degrees of freedom in motion and small pitch angles, the equation of motion can be written as (Fang et al. 2005):

$$X = m(\dot{u} - vr)$$

$$Y = m(\dot{v} + ur)$$

$$Z = m\dot{w}$$

$$K = I_{xx}\dot{p} - I_{xx}qr$$

$$M = I_{yy}\dot{q} + I_{xx}pr$$

$$N = I_{zz}\dot{r} - I_{xx}pq \qquad (7)$$

where X, Y and Z are external forces with respect to surge, sway and heave and K, M and N are external moments with respect to roll, pitch and yaw respectively. The terms m and I denote the total mass and moment of inertia. In this equation, the non-diagonal elements of moments of inertia matrix are neglected as they are small comparing to the diagonal terms and the vessel assumed to be symmetrical in port and starboard.

The left side of Equation 7 can be expressed as:

$$X = X_R + X_{HS} + X_P + X_A$$

$$Y = Y_R + Y_{HS} + Y_A$$

$$Z = Z_{HS} + Z_A + Z_{G-B}$$

$$K = K_R + K_{HS} + K_A + K_{G-B}$$

$$M = M_{HS} + M_P + M_A + M_{G-B}$$

$$N = N_R + N_{HS} + N_A \qquad (8)$$

where subscripts R, HS, P, A and G-B denote rudder forces, steady hydrodynamic forces, propulsion, added mass and combined gravity and buoyancy forces, respectively. Later in this chapter, the evaluation and calculation of the forces and moments acting on the vessel are described in detail.

3.2 Hydrodynamic forces acting on ship's hull

Hydrodynamic forces acting on ship hull are expressed as:

$$X_H = \frac{1}{2}\rho L d U^2 X'_H(\psi, r')$$

$$Y_H = \frac{1}{2}\rho L d U^2 Y'_H(\psi, r')$$

$$Z_H = \frac{1}{2}\rho L d U^2 Z'_H(\psi, r')$$

$$K_H = \frac{1}{2}\rho L^2 d U^2 K'_H(\psi, r')$$

$$M_H = \frac{1}{2}\rho L^2 d U^2 M'_H(\psi, r')$$

$$N_H = \frac{1}{2}\rho L^2 d U^2 N'_H(\psi, r') \quad (9)$$

where $X'_H, Y'_H, Z'_H, K'_H, M'_H$ and N'_H are expressed as polynomial functions of ψ and the non-dimensionalized yaw rate r' by rL/U (Yasukawa & Yoshimura 2014). However, for the case of this study several experiments were conducted in various yaw angles, so hydrodynamic coefficients of forces acting on the ship hull are expressed only as a function of the yaw angle. Non-dimensional damping coefficients are then added to the model to take the effects of heave, roll, pitch and yaw rate into consideration. The magnitude of these coefficients were estimated during a trial and error procedure, to match the maneuvering behavior of the vessel in free-running trials. To achieve more

reliable and accurate estimation of damping coefficients, a Planar Motion Mechanism can be employed during the towing experiments.

$$X_H^{'} = X_{\psi\psi\psi\psi}^{'}\psi^4 + X_{\psi\psi\psi}^{'}\psi^3 + X_{\psi\psi}^{'}\psi^2 + X_{\psi}^{'}\psi + X_0^{'}$$

$$Y_H^{'} = Y_{\psi\psi\psi}^{'}\psi^3 + Y_{\psi\psi}^{'}\psi^2 + Y_{\psi}^{'}\psi$$

$$Z_H^{'} = Z_{\psi\psi}^{'}\psi^2 + Z_{\psi}^{'}\psi + Z_0^{'}$$

$$K_H^{'} = K_{\psi\psi\psi}^{'}\psi^3 + K_{\psi\psi}^{'}\psi^2 + K_{\psi}^{'}\psi$$

$$M_H^{'} = M_{\psi\psi\psi\psi}^{'}\psi^4 + M_{\psi\psi\psi}^{'}\psi^3 + M_{\psi\psi}^{'}\psi^2 + M_{\psi}^{'}\psi + M_0^{'}$$

$$N_H^{'} = N_{\psi\psi\psi}^{'}\psi^3 + N_{\psi\psi}^{'}\psi^2 + N_{\psi}^{'}\psi \qquad (10)$$

where $X'_{\psi\psi\psi\psi}$, $X'_{\psi\psi\psi}$, $X'_{\psi\psi}$, X'_{ψ}, X'_0, $Y'_{\psi\psi\psi}$, $Y'_{\psi\psi}$, Y'_{ψ}, $Z'_{\psi\psi}$, Z'_{ψ}, Z'_0, $K'_{\psi\psi\psi}$, $K'_{\psi\psi}$, K'_{ψ}, $M'_{\psi\psi\psi\psi}$, $M'_{\psi\psi\psi}$, $M'_{\psi\psi}$, M'_{ψ}, M'_0, $N'_{\psi\psi\psi}$, $N'_{\psi\psi}$ and N'_{ψ} are the hydrodynamic derivatives of the maneuvering.

The hydrodynamic derivatives shown above were obtained by conducting towing experiments which are described in detail in chapter 4 of this thesis. Table 1 shows a summary of the result:

Table 1- Non-dimensional hydrodynamic derivatives of the hull

$X'_{\psi\psi\psi\psi}$	-8.84	$K'_{\psi\psi\psi}$	63.48
$X'_{\psi\psi\psi}$	0.211	$K'_{\psi\psi}$	-0.393

$X'_{\psi\psi}$	7.05	K'_{ψ}	-36.38
X'_{ψ}	-0.131	$M'_{\psi\psi\psi\psi}$	-58.19
X'_{0}	0.0946	$M'_{\psi\psi\psi}$	-0.506
$Y'_{\psi\psi\psi}$	-8.93	$M'_{\psi\psi}$	38.65
$Y'_{\psi\psi}$	0.199	M'_{ψ}	0.00268
Y'_{ψ}	3.56	M'_{0}	0.123
$Z'_{\psi\psi}$	2.83	$N'_{\psi\psi\psi}$	0.402
Z'_{ψ}	0.196	$N'_{\psi\psi}$	0.0658
Z'_{0}	0.0966	N'_{ψ}	-0.382

3.3 Evaluation of rudder forces and moments

Forces and moments acting on a ship by the rudder can be expressed as:

$$X_R = \frac{1}{2}(\rho A_R U_R^2 \sin\alpha_R)\sin\delta\, X'_R$$

$$Y_R = \frac{1}{2}(\rho A_R U_R^2 \sin\alpha_R)\cos\delta\, Y'_R$$

$$K_R = \frac{1}{2}(\rho A_R L U_R^2 \sin\alpha_R)\cos\delta\, K'_R$$

$$N_R = \frac{1}{2}(\rho A_R L U_R^2 \sin\alpha_R)\cos\delta\, N'_R \qquad (11)$$

where A_R is the profile area of the movable part of the marine rudder, U_R is the resultant inflow velocity to the rudder, α_R is the effective inflow angle to the rudder, and X'_R, Y'_R, K'_R and N'_R are non-dimensional hydrodynamic coefficients for maneuvering and mainly represent the hydrodynamic interaction between the rudder and hull.

The hydrodynamic coefficients shown above are empirically expanded and described for conventional marine vessels, i.e. the one introduced by Hirano (1980), but for the case of the propelled SPAR vessel, there is no empirical formulation to describe the coefficients. Hence, in this study rudder forces and moments are assumed to be a linear function of A_R, U^2, α_R, δ, L and the hydrodynamic coefficients of the rudder.

These coefficients are evaluated by comparing the results of towing experiments at various rudder angles. When the effective inflow angle to the rudder is zero, rudder forces and moment are expected to be zero and the ship hull is responsible for the total measured forces. In the same situation, as the rudder angle changes, rudder forces and moments are assumed to be the cause of any variations in results.

Figures 3 to 6 show the effect of rudder angle on the total hydrodynamic forces and moments in the towing experiments.

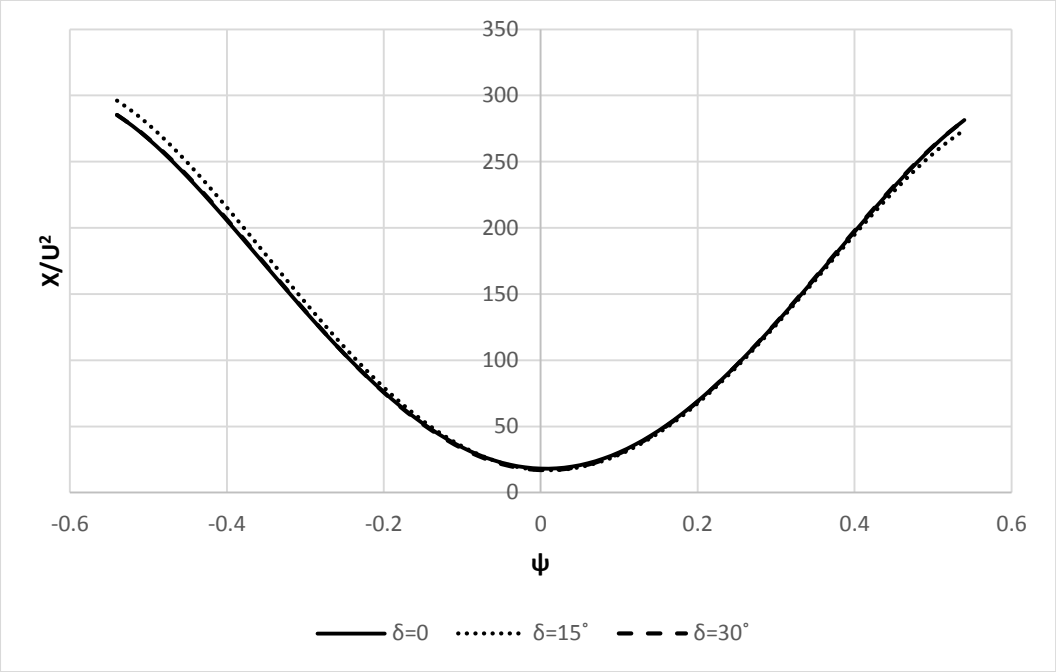

Figure 4- Surge resistance force vs. yaw angle at various rudder angles

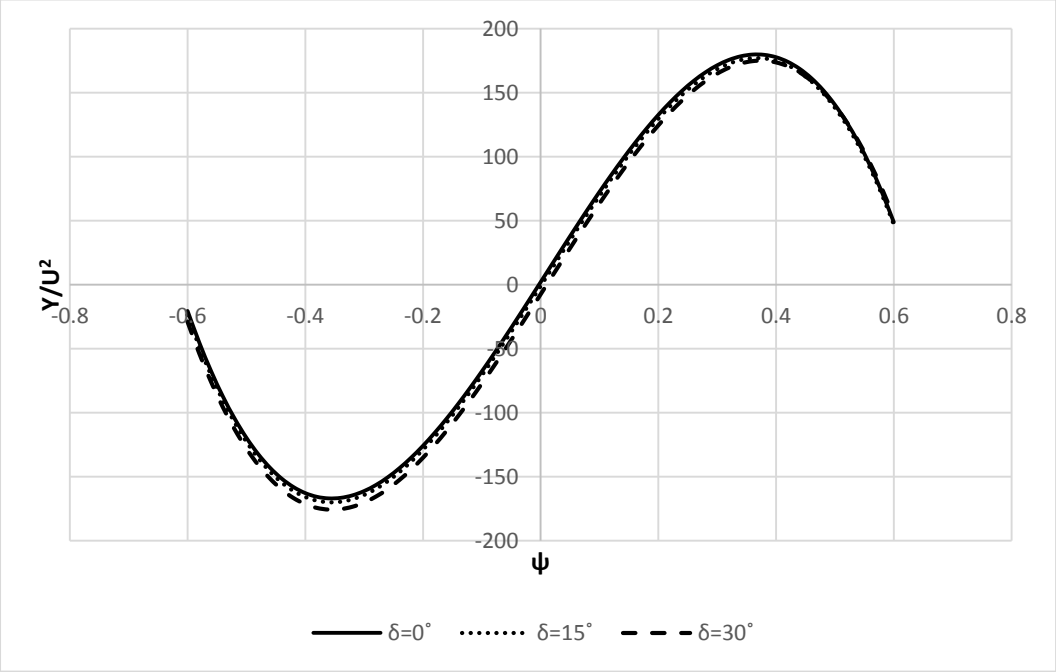

Figure 5- Sway resistance force vs. yaw angle at various rudder angles

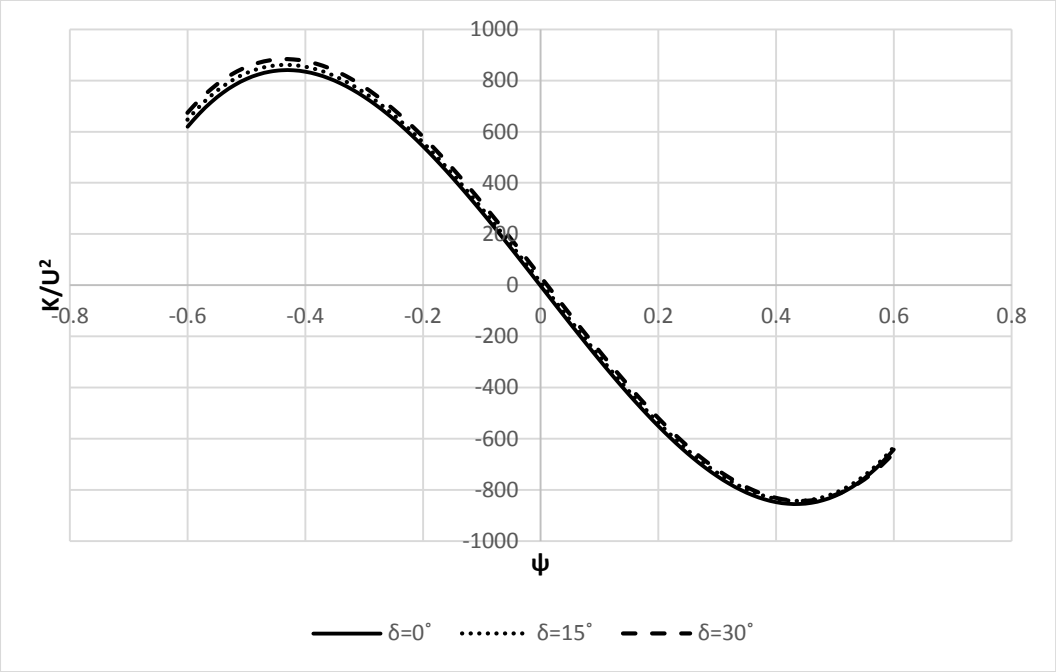

Figure 6- Roll resistance moment vs. yaw angle at various rudder angles

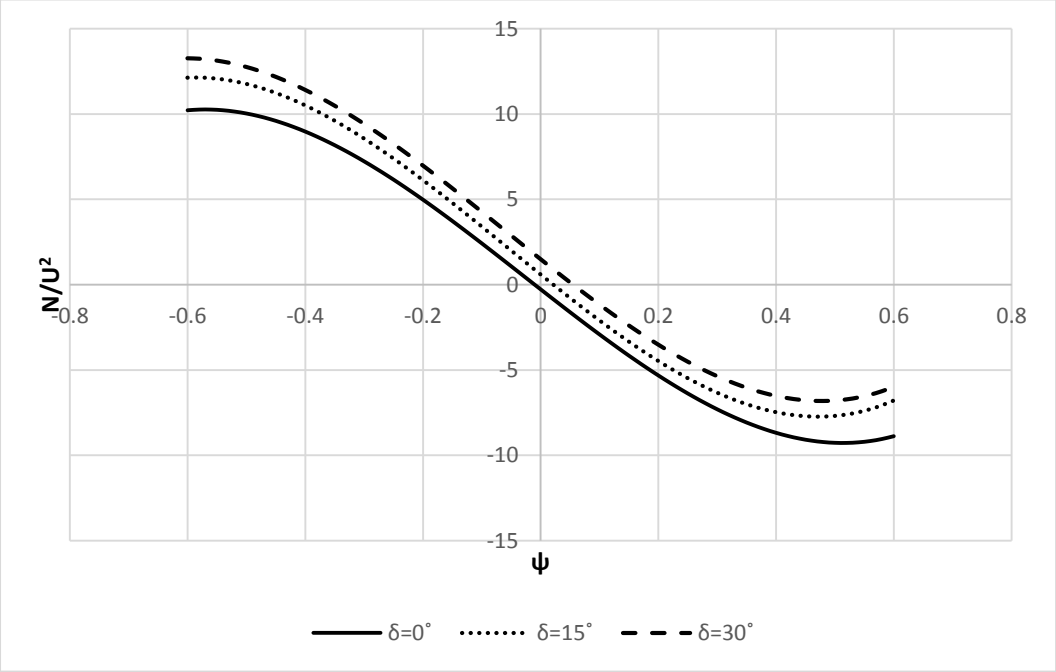

Figure 7- Yaw resistance moment vs. yaw angle at various rudder angles

The calculated magnitude of rudder forces lies on the left side of equation 11. On the right side, values of A_R, U^2, α_R, δ and L could be determined in each experimental setup, so the only unknown parameters in each equation are the non-dimensional hydrodynamic coefficients of the rudder X'_R, Y'_R, K'_R and N'_R. The values of these coefficients were curve fitted to the experimental results with the lowest achievable deviation.

3.4 Propeller hydrodynamic force

The propelled SPAR model was fitted with a Wageningen B-series 4 blade propeller B4-70. Figure 7 shows the propeller and rudder components setup on the model strut and the propeller specifications are presented in Table 2.

Table 2- Propeller specifications

Designation	Modified B-Series
D (Diameter)	0.107m
P/D (Pitch/Diameter)	1.1
A_E	0.7
z	4

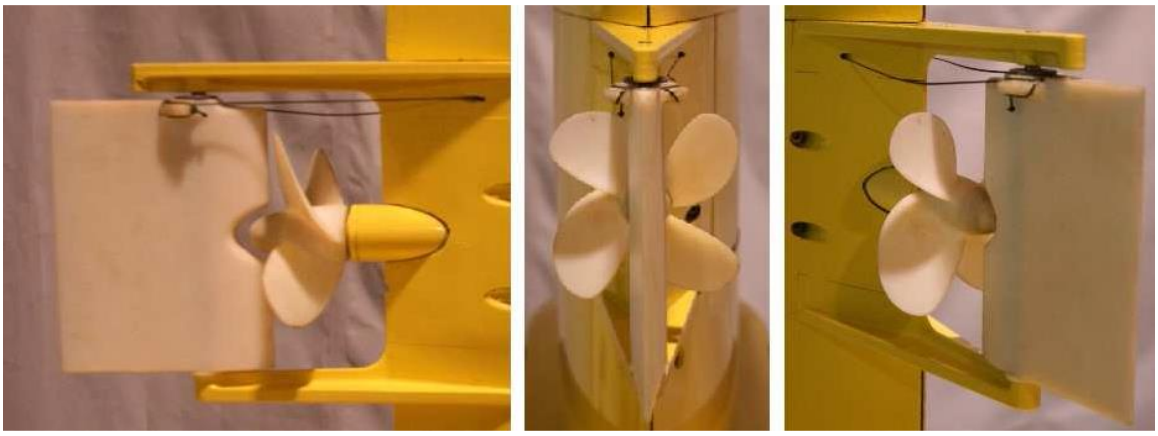

Figure 8- Rudder and propeller setup

The hydrodynamic force due to propulsion of a marine vessel with a single propeller is expressed as a fraction of the propeller thrust:

$$X_P = (1 - t_P)T \qquad (12)$$

The thrust deduction factor t_P is assumed here to be constant at 0.1 in any given propeller load. Propeller thrust T is calculated as:

$$T = \rho n_P^2 D_P^4 K_T(J_P) \qquad (13)$$

where n_P is the propeller revolution in rps, D_P is the propeller diameter, and the thrust coefficient K_T is defined as a quadratic polynomial function of the propeller advance ratio J_P. The thrust coefficient of the propeller at the zero forward speed test was found to be 0.6 (ExtremeOcean Innovation Inc. 2013) which is 20% higher than the expected value of 0.5 and reaches zero at an advance coefficient of 1.17.

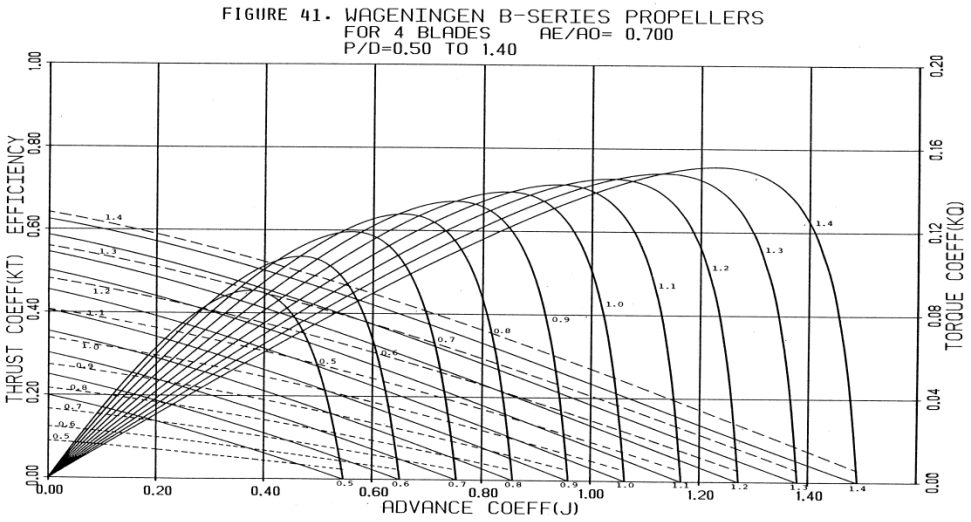

Figure 9- B-series Wageningen propeller chart, from (Bernitsas et al. 1981)

$$K_T = -0.115J_P^2 - 0.379J_P + 0.6$$

$$J_P = \frac{V_A}{nD} \qquad (14)$$

where V_A denotes the speed of advance. In the calculation of propeller force, the effect of steering on propeller thrust is neglected as the propeller was not installed during the experiments.

As the propeller is at a different height from the vertical center of gravity, it also produces a trimming moment around the CoG equivalent to propeller thrust multiplied by the vertical distance betweenthe CoG and propeller hub. As the propulsion force is applied at the latitudinal center of the vessel and parallel to the longitudinal vector of it, roll and yaw moments can be considered zero.

3.5 Restoring forces

Gravity and buoyancy forces applied to a floating body are expressed in a matrix form as:

$$\begin{Bmatrix} X_{G-B} \\ Y_{G-B} \\ Z_{G-B} \\ K_{G-B} \\ M_{G-B} \\ N_{G-B} \end{Bmatrix} = -[C] \times \begin{Bmatrix} \xi \\ \eta \\ \zeta \\ \phi \\ \theta \\ \psi \end{Bmatrix} \tag{15}$$

in which elements C_{33}, C_{34}, C_{35}, C_{43}, C_{44}, C_{45}, C_{53}, C_{54} and C_{55} are the only non-zero elements of the matrix C. In a small perturbation, all the diagonal terms are negative, which indicates that Gravity-Buoyancy forces are opposing the perturbations (Lewandowski 2004). Center of Floatation (CoF) of a freely floating body lies at the center of its water plane. Equation 16 expresses the restoring forces and moments of a body with port-starboard symmetry.

$$Z_{G-B} = -\rho g A_{WP} \zeta + \rho g S_x \theta$$

$$K_{G-B} = -\rho g \left[\nabla_0 (z_G - z_B) + S_{yy}\right] \phi$$

$$M_{G-B} = -\rho g [\nabla_0 (z_G - z_B) + S_{xx}] \theta + \rho g S_x \zeta \tag{16}$$

where A_{WP} is the water plane area, S_x, S_{xx}, and S_{yy} are water plane moments, ∇_0 is volume of displacement, z_G is the height of the CoG and z_B is the height of the center of buoyancy.

In order to estimate values of A_{WP}, S_x, S_{xx}, S_{yy}, ∇_0, z_G and z_B, a detailed 3D CAD model of the vessel was built. Figure 9 shows a rendering of the 3D model beside a picture of the physical model. Table 3 shows the calculated values of the restoring force parameters from the CAD model.

Figure 10- Rendering of the CAD model vs the physical model

Table 3- Calculated parameters of the model vessel

A_{WP}	29365mm^2	S_{xx}	2.2E-5m^4	z_B	95mm
∇_0	0.0666m^3	S_{yy}	2.5E-4m^4	z_G	0

3.6 Added mass and added moment of inertia

When a body accelerates in a fluid, it experiences a hydrodynamic force opposing the acceleration due, and proportional, to acceleration. This force can be explained as the amount of force needed to accelerate the fluid surrounding the body. The added mass and added moment of inertia are defined as matrix *A*, where A_{ij} indicates the "magnitude of the hydrodynamic force in direction *i* due to unit acceleration in direction *j*" where subscripts *i* and *j* range from 1 to 6 and correspond the surge, sway, heave, roll, pitch and yaw directions (Lewandowski 2004).

The added mass forces are considered negative because they oppose the acceleration. Unit of A_{ij} is the mass for *i* and *j* between 1 and 3, the moment of inertia for *i* and *j* between 4 and 6 and the mass×length for all other cases. The added mass matrix is composed of 36 elements; however, it is a symmetrical matrix for all floating objects so $A_{ij}=A_{ji}$. It can be shown that the added mass forces and moments can be expressed as (Newman 1977):

$$F_{AM} = -\sum_{j=1}^{6}\left(\dot{U}_j A_j + U_j \Omega \times A_j\right) \qquad (17)$$

$$M_{AM} = -\sum_{j=1}^{6}\left(\dot{U}_j A_j + U_j \Omega \times A_j + U_j U \times A_j\right) \qquad (18)$$

For a body with port-starboard symmetry, it can be shown that:

$A_{32}=A_{34}=A_{36}=A_{52}=A_{54}=A_{56}=A_{12}=A_{14}=A_{16}=0$

Due to the symmetry property of the matrix:

$A_{23}=A_{43}=A_{63}=A_{25}=A_{45}=A_{65}=A_{21}=A_{41}=A_{61}=0$

Expanding Equations 17 and 18 and considering the symmetry of the body and added mass matrix, the final equations of added mass and added moments of inertia due to small accelerations are:

$$X_{AM} = -A_{11}\dot{u} - A_{13}\dot{w} - A_{15}\dot{q}$$

$$\mathbf{Y_{AM}} = -\mathbf{A_{22}\dot{v}} - \mathbf{A_{24}\dot{p}} - \mathbf{A_{26}\dot{r}} \qquad (19)$$

$$Z_{AM} = -A_{31}\dot{u} - A_{33}\dot{w} - A_{35}\dot{q}$$

$$X_{AM} = -A_{42}\dot{v} - A_{44}\dot{p} - A_{46}\dot{r}$$

$$\mathbf{X_{AM}} = -\mathbf{A_{51}\dot{u}} - \mathbf{A_{53}\dot{w}} - \mathbf{A_{55}\dot{q}} \qquad (20)$$

$$X_{AM} = -A_{61}\dot{v} - A_{63}\dot{p} - A_{65}\dot{r}$$

Evaluation of added mass coefficients is obtained using the boundary integral equation method, also known as the panel method. The outer shell of the CAD model was exported to WAMIT software (Anon 2015b) . To estimate the fluid forces, potential flow theory is considered for the relationship between fluid pressure and interface acceleration, where the velocity potential function satisfies the Laplace equation (Bašić & Parunov 2013). Table 4 shows the added mass coefficients for the vessel calculated by this method.

Table 4- Non-dimensional added mass coefficients

ADDED-MASS COEFFICIENTS					
I	J	A'(I,J)	I	J	A'(I,J)
1	1	3.34E-03	4	2	2.92E-02
1	3	-6.04E-05	4	4	1.73E-02
1	5	-1.95E-03	4	6	8.56E-04
2	2	4.95E-02	5	1	-1.97E-03
2	4	2.92E-02	5	3	4.48E-04
2	6	1.35E-03	5	5	5.62E-03
3	1	-4.91E-05	6	2	1.38E-03
3	3	5.13E-02	6	4	8.74E-04
3	5	4.71E-04	6	6	2.56E-03

The added mass coefficients are non-dimensionalized by ρL^k where:

$k = 3$ for $(i; j = 1; 2; 3)$

$k = 4$ for $(i = 1; 2; 3; j = 4; 5; 6)$ *or* $(i = 4; 5; 6; j = 1; 2; 3)$

$k = 5$ for $(i; j = 4; 5; 6)$

4 Experimental procedure

4.1 Instrumentation

Scale model experiments were conducted to measure the hydrodynamic forces on the vessel including the rudder forces at various fixed yaw angles and various forward speeds. The purpose of these experiments was to obtain the hydrodynamic coefficients of the hull and the rudder for the numerical maneuvering model. This chapter introduces equipment and devices used for the experiments.

4.1.1 Dynamometer

A global dynamometer was used to measure forces and moments on the model vessel, propeller or any other instrument connected to its arm. The global dynamometer used as the force measurement device in this project was a global dynamometer designed and built by Mr. Andrew MacNeill, a former Master's student in Ocean and Naval Architectural Engineering, as a part of his master's degree project.

The dynamometer is composed of 6 individual 1000 lbs (4447 N) load-cells mounted on an adaptor frame. With the design of the adaptor and dynamometer frame completed in detail, the flex links and their mounts were added to the main frame.

In order to achieve design goals within limitations, the materials used in the majority of the dynamometer were mild steel plate and thin walled square tubing. The main thought behind the design was to gain an optimum design which would provide both maximum

stiffness and lightness at the same time. In addition, to ease the machining and fabrication process, bolt connections are used widely in the design (MacNeill 2011).

Figure 11- NSERC global dynamometer

4.1.2 Flex links

The forces applied to the live frame are transferred to the load cells through flex links. The main purpose of using the flex links is to transfer forces only from the primary direction to the load cells. The links are stiff in the axial direction but flexible in the lateral direction and thus they do not transmit side loads to the load cells as the frame moves slightly under load or moment. This ensures that the measured loads in each direction are not influenced by small motions in other directions (known as crosstalk).

Moreover, the design of the flex links ensures that when the amount of forces or moments applied to the frame exceeds the capacity of the load cells, the flex link attached to the load cell will break and prevent damage to the load cell.

The material selected for the flex link was 17-4 PH stainless steel. The following is the specification of the 17-4 PH:

Table 5- Chemical properties of the flex links material (Anon 2015a)

TYPE	Cr	Ni	Cu	Cb + Ta	C	Mn	P	S	Si
17-4 (H900)	min: 15.0	min: 3.0	min: 3.0	min: 0.15	0.07	1	0.04	0.03	1
	max: 17.5	max: 5.0	max: 5.0	max: 0.45	max	max	max	max	M

Table 6- Mechanical properties of the flex links material (Anon 2015a)

Hardening or Precipitation Treatment at 900°F						
Thickness,	**Ultimate Tensile**	**0.2% Yield**	**Elongation % in 2" min.**	**Reduction in Area min. %**	**Hardness,**	**Hardness, Brinell,**
inches	**Strength, ksi min.**	**Strength, ksi min.**			**Rockwell,**	**min. / max.**
					min. / max	
Under 0.1875"	190	170	5	—	C40 – C48	—
0.1875" to 0.625"	190	170	8	25	C40 – C48	388 / 477
0.625" to 4.0"	190	170	10	30	C40 – C48	388 / 477

4.1.3 Load cells

As mentioned above, six individual load cells are installed on the fixed frame, three, two, and one load cells in Z, X and Y directions respectively. The capacity of each load cell is 1000 lbs.

All flex links and load cells are designed with the ability of being installed or removed independently from other assemblies (MacNeill 2011).

4.1.4 Adjustable towing arm

The NSERC global dynamometer was initially designed to measure forces on a podded propeller. As the purpose of this research is to study forces applied to a model vessel, a few adjustments needed to be made to the instruments.

In order to connect the model vessel to the live frame of the dynamometer, an adjustable towing arm was designed (by Cotrim Ferreira Oliveira Botelho, a Brazilian exchange program student at the time) and built by MUN Technological Services. The aluminum towing arm consists of a rotatable circular plate bolted to a cubic hollow column. The whole setting is secured to the live frame of the dynamometer with a thick rectangular plate. The other end of the column is connected to the vessel with four stainless steel bolts.

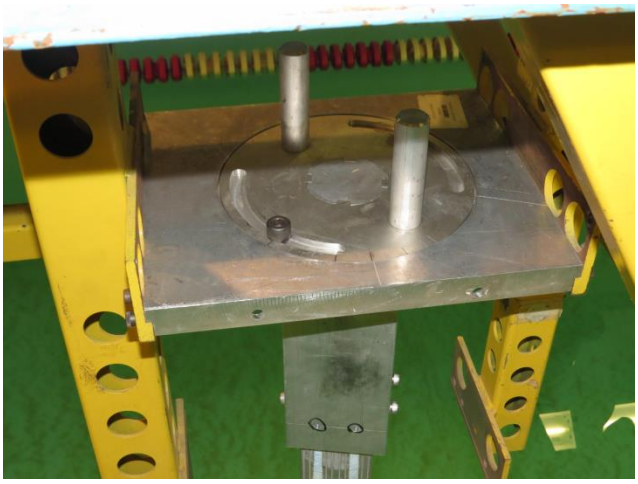

Figure 12- Adjustable towing arm

The design of the arm provides a fixed roll and pitch angle at zero degrees, but an adjustable yaw angle between 40° to -40°.

4.1.5 Data Acquisition System

The process of measuring an electrical or physical phenomenon such as voltage, pressure or current is called data acquisition (DAQ) (National Instruments 2015). The DAQ system consists of:

1- Sensors: which are the six load cells described above.

2- DAQ measurement hardware: The NI cDAQ-9178 (which is an eight-slot National Instruments (NI) CompactDAQ chassis) was used as the measurement hardware. This is a portable chassis that can be combined with up to eight NI C series I/0 modules for a custom analog input, analog output, digital I/O, and counter/timer measurement system (National Instruments 2015).

Figure 13- NI cDAQ-9178 DAQ chassis

The following are the highlights of the technical specification of the NI cDAQ-9178 measurement DAQ chassis:

Table 7- Technical specification of the NI cDAQ-9178 DAQ chassis

Input FIFO size	127 samples per slot
Maximum sample rate	Determined by the C Series I/O module(s)
Timing accuracy	50 ppm of sample rate
Timing resolution	12.5 ns
Number of channels supported	Determined by the C Series I/O module(s)
Onboard regeneration	16

3- Universal analogue input: Two NI 9219 analogue input modules were used to digitize voltages after excitation. Three load cells were connected to each module to cover signals from all six load cells. Table 8 shows highlights of technical specifications of the NI 9219 analogue input module:

Table 8- Technical specifications of NI 9219 analogue input module

Number of channels	4 analog input channels
ADC resolution	24 bits
Type of ADC	Delta-sigma (with analog prefiltering)
Sampling mode	Simultaneous
Type of TEDS supported	IEEE 1451.4 TEDS Class II (Interface)

Figure 14- NI 9219 analogue input module

4- Industrial controller: the NI 3100 industrial controller is an industrial PC which incorporates a 1.06 GHz Intel Celeron M processor. This PC is connected to the measurement hardware via Hi-Speed USB connection. This computer reads and stores digitized data from the load cells.

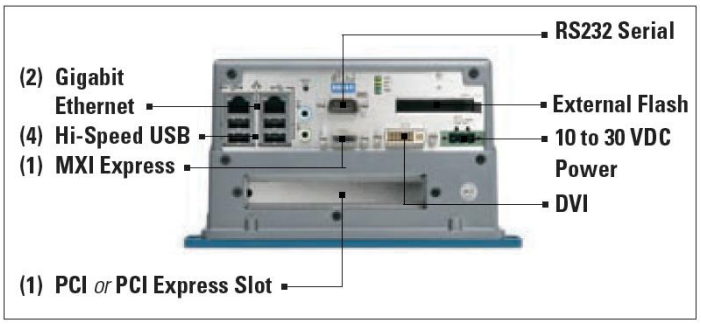

Figure 15- NI 3100 industrial controller

PC-based DAQ systems, like the one used during these experiments provide high power, connectivity capabilities, flexibility and display options (National Instruments, 2015).

4.2 Calibration

Section describes the process of calibrating six axial load cells and the towing carriage during the model experiments.

4.2.1 Load cell calibration

Each load cell was calibrated individually in an un-installed condition. As the factory specification sheet of the load cells states that the slope of the trend line of the load cells is identical for tension and compression, calibrating them in only pull mode was adequate. To achieve pure tension force on each load cell, the load cell was vertically installed and fixed on a rigid frame, and a small steel adaptor was used to install a hanger on it.

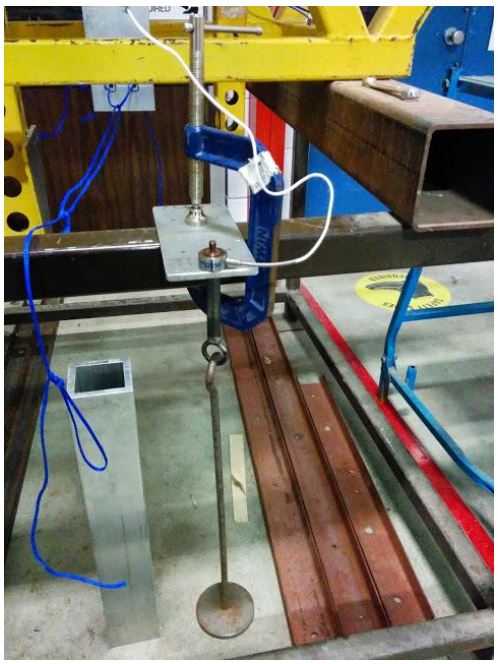

Figure 16- Loading and unloading assembly of load cells

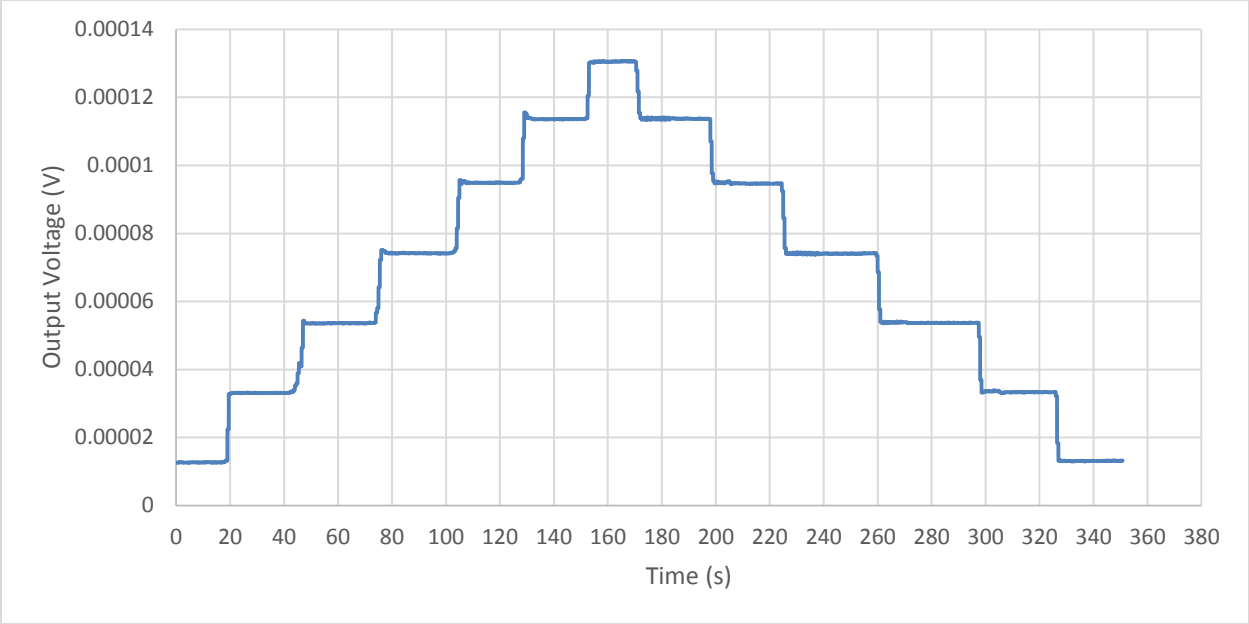

Figure 17- Load cell Y1 time series plot

Table 9- Average output voltage in stable regions of loading and unloading of load cell Y1

Test Number	Added weight (g)	Total weight (g)	Average voltage (µV)
1	884	884	12.694
2	5032	5916	33.100
3	5036	10952	53.599
4	5019	15971	74.159
5	5031	21002	94.913
6	4577	25579	113.572
7	4018	29597	130.544
8	-4018	25579	113.741
9	-4577	21002	94.656
10	-5031	15971	74.077
11	-5019	10952	53.712
12	-5036	5916	33.331
13	-5032	884	13.161

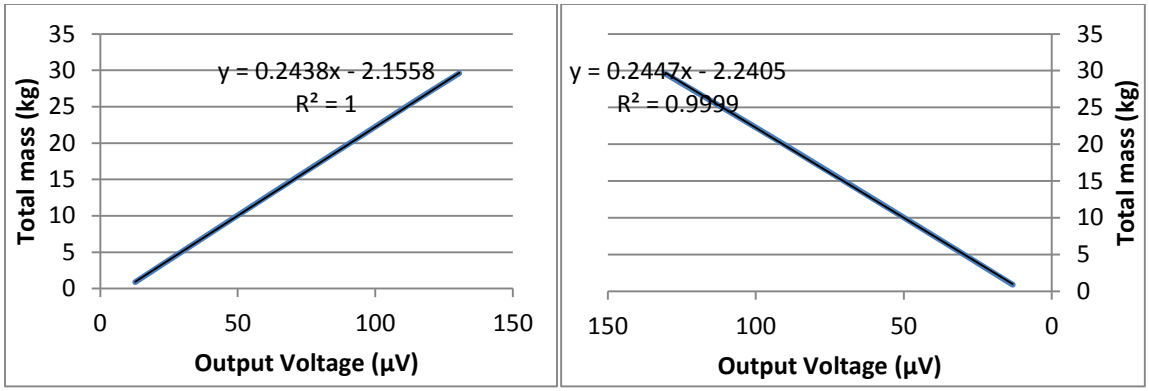

Figure 18- Calibration plot for loading (left) and unloading (right) load cell Y1

The value of R^2 for the linear trend line is 0.9999, which means choosing a linear calibration line for the load-cells is reliable. As the slope of the trend line for loading and unloading is slightly different, the average of 0.2442 was chosen as the calibration coefficient.

To validate the calibration coefficient, two verification experiments were conducted. In each experiment a known amount of weight was hung on the load cell. Then, the predicted value from applying the coefficient to the average voltage was compared to the actual weight.

Table 10- Verification result for calibration of load cell Y1

Weight(g)	Voltage(V)	Prediction(g)	Error (%)
10934	5.38E-05	10933.6	0.004
21001	9.55E-05	21127.6	0.603

For all other load cells the same procedure for calibration and validation is implemented. The calibration and validation data and diagrams for the 5 remaining load cells are shown in the Appendix A.

4.2.2 Towing carriage velocity calibration

The towing carriage in the MUN Fluids lab is widely used for academic and industrial purposes, so it is professionally calibrated on an annual basis to ensure precision in velocity during experiments. It has been calibrated again just before the beginning of the experiments. The velocity of the carriage in each run is measured by counting the rotation time of the carriage axle with an optical (laser) sensor. The rpms are then converted to velocity and compared to the output voltage of the velocity sensor.

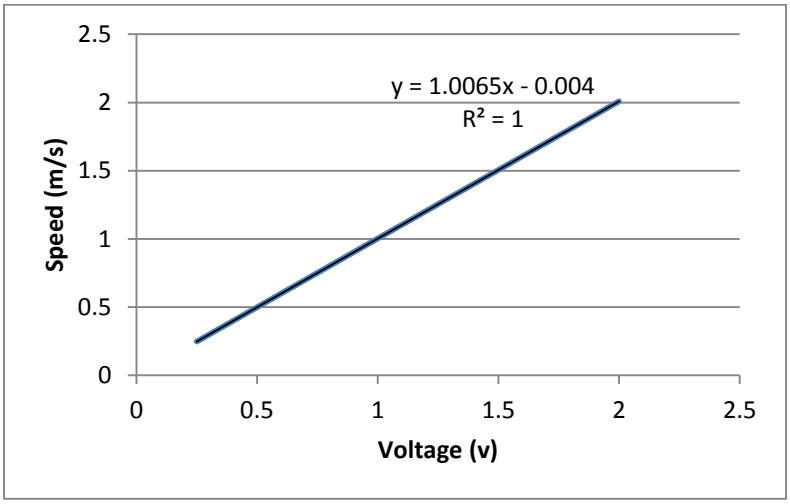

Figure 19- Towing carriage velocity calibration data

4.2.3 Assembled dynamometer reliability validation

In section 4.2.1 of this thesis, the procedure of the calibration and validation of each individual load-cells are described. To validate that the total force on the live frame of the

dynamometer, conform the summation of the forces on individual load cells, pull experiment on the assembled dynamometer with 5 known weights on the three axial directions was conducted. Figure 20 shows the results of the pulling experiment in the *x* direction:

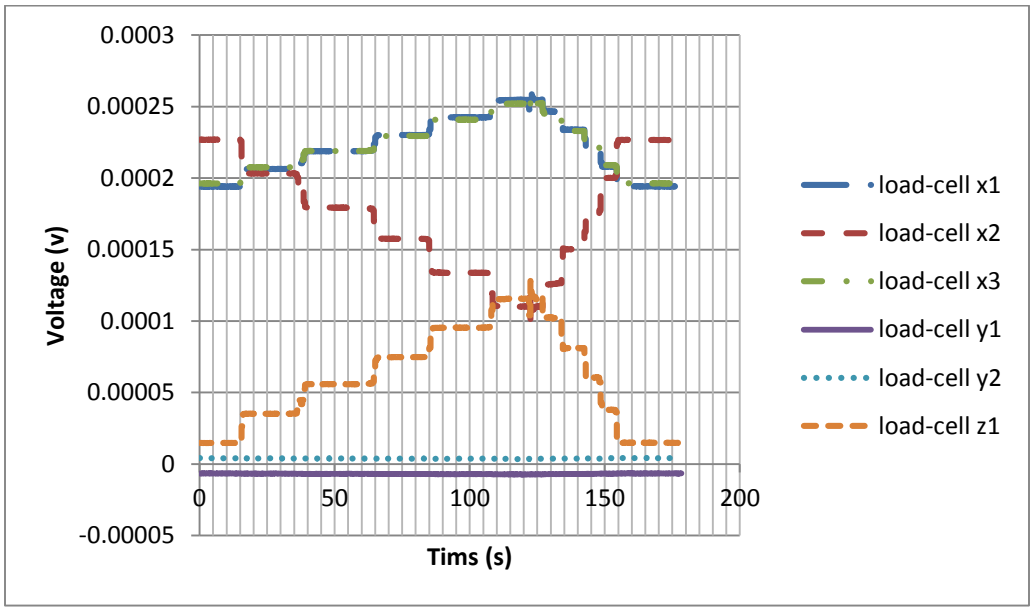

Figure 20- Assembled Dynamometer pull on experiments results in x direction

The assembled dynamometer pulling experiments confirm the compliance between the estimated forces (from the load-cells outputs) and applied forces for all the directions. The errors for the estimations are in the range of 1% for *x* direction, 3% for *y* direction and 4% for *z* direction.

4.3 Experimental setup

The experimental setup for the towing test of the model is shown in Figure 20. More details on the installation are referred to in MacNeill (2011).

- Fixed frame: the fixed frame is set on the towing rail on the carriage and provides secured rigid support for the rest of instrumentation. This frame is not adjustable and remained parallel to the tank line for all the experiments.
- Live frame: the live frame is secured by the fixed frame and houses all of the measuring instrumentation including load cells and flex links. This frame was fixed to the upper frame to avoid any bending or failure on the flex links. After putting the dynamometer on the towing tank, solid connections were removed to divert all forces applied to the model load cells.
- Towing carriage: the towing carriage located in the MUN Fluids lab is an electronic powered carriage capable of towing models up to maximum of 5 m/s; however due to the limitation on the maximum force on the dynamometer, the maximum towing velocity was selected as 2.5 m/s.
- Wave tank: the experiments were conducted in the 52 meter long wave tank in the MUN Hydraulic Lab.

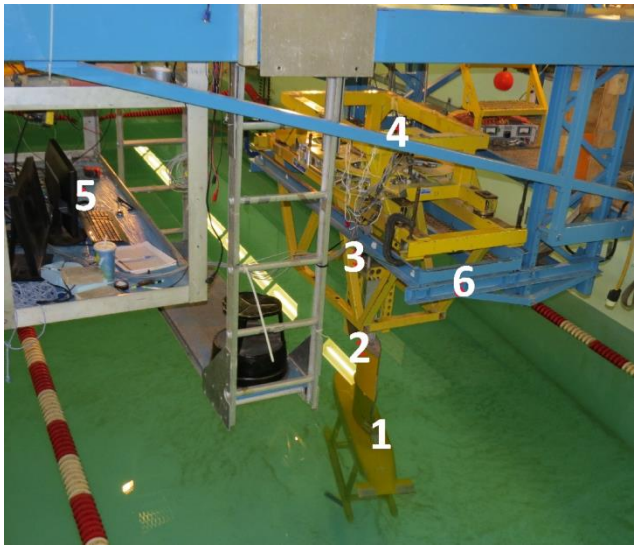

Figure 21- Experimental setup for towing test

1- Model vessel

2- Connecting arm

3- Live frame

4- Fixed frame

5- Data acquisition system

6- Carriage fixed towing rail

4.4 Experiments

As mentioned above, the direct output of the experiments are voltages read from the load cells in a time domain. These voltages represent the amount of force applied to a load cell at time *t*. The data acquisition frequency during all the experiments was set to 50 Hz.

This rate was selected to ensure that enough data points were recorded to observe all the fluctuations in forces at any specific time.

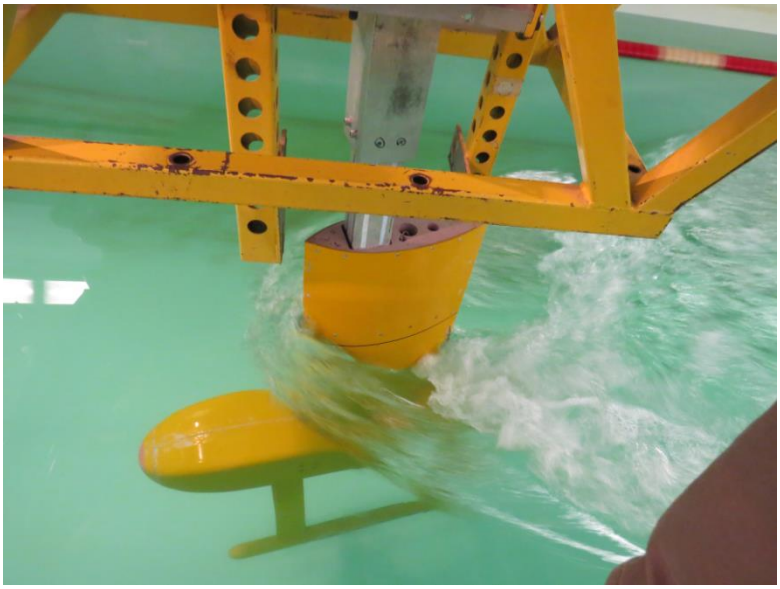

Figure 22- Experiment # 19 water surface

The first step to analyse the data is to average the output voltage of each load cell over the steady state process.

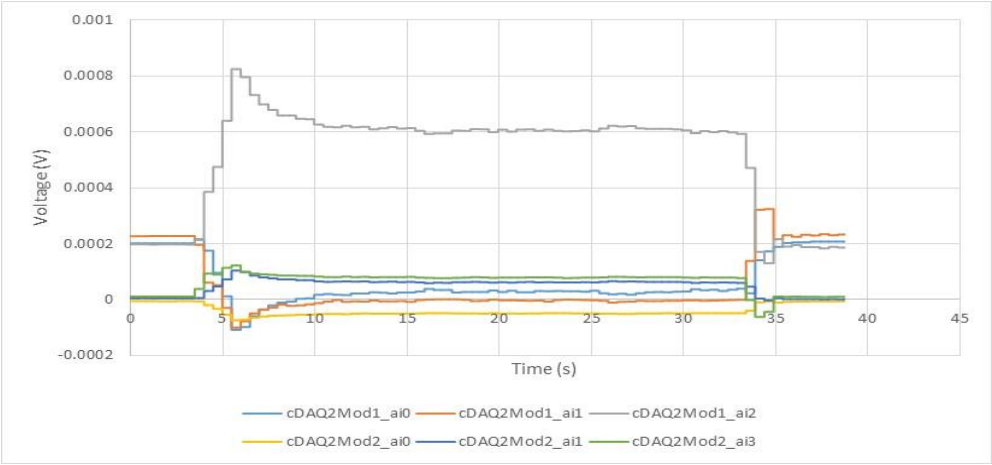

Figure 23- Experiment # 50 load cell voltage data

Figure 22 demonstrates the raw results of experiment 1. The towing carriage in this experiment was stopped in the first 4.5 seconds of the experiments. It then started moving forward and reached the maximum velocity of 0.5 m/s at t=6s. It moved with constant velocity of 0.5 m/s for about 50 seconds and then stopped at t=56s.

The goal of this experiment was to measure the forces applied to the vessel at a velocity of 0.5 m/s, so the output voltages of the load cells were averaged between the t=20s and t=50s. Then the tare value, which is the average voltage read from t=0s to t=4s, when the vessel was stopped, was subtracted from them. The taring procedure ensures that the outcome does not include any initial forces on the load cell resulting from the weight of the instrumentations or any other external forces; it only describes forces applied to the vessel due to forward displacement.

These subtracted average output voltages were then converted to forces on the load cells, using the calibration coefficient described and calculated earlier.

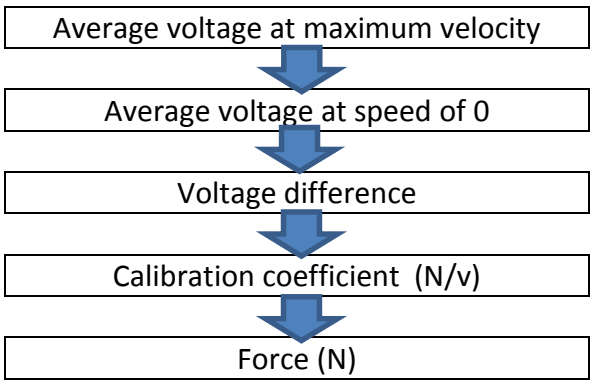

Table 11- Calculation of force on individual load cells in experiment #1

load cell	z1	z2	z3	y1	y2	x1
Average voltage at speed of 0.5 m/s	1.57E-04	1.66E-04	3.01E-04	-1.65E-05	2.04E-05	2.86E-05
Average voltage at speed of 0	1.99E-04	2.26E-04	1.97E-04	-5.75E-06	6.14E-06	1.14E-05
Voltage difference	4.22E-05	6.02E-05	-1.04E-04	1.07E-05	-1.43E-05	-1.72E-05
Calibration coefficient (kg/μv)	2.32E-01	2.28E-01	2.19E-01	2.44E-01	2.23E-01	2.47E-01
Calibration coefficient (N/v)	2.27E+06	2.24E+06	2.15E+06	2.40E+06	2.18E+06	2.43E+06
Force (N)	95.84	134.75	-222.78	25.66	-31.16	-41.63

Forces on the load cells are then transferred to forces and moments applied to the model's center of gravity.

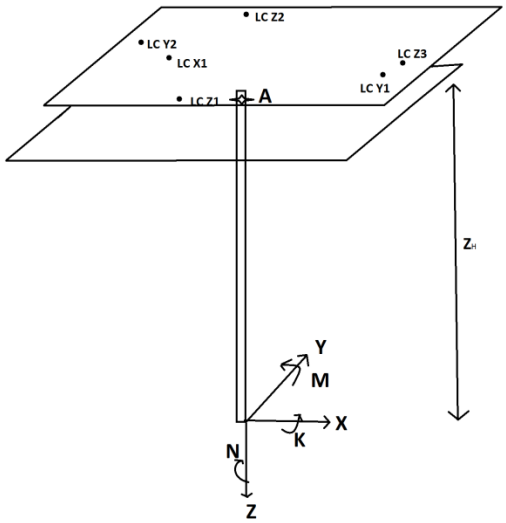

Figure 24- Geometry of the model CoG related to the dyno

As both of the frames and the towing arm were fixed, the acceleration and thus, the sum of the forces applied to point A in each direction was zero.

$$\Sigma F_x=0 \rightarrow X+F_{X1}=0 \rightarrow X=-F_{X1}$$

$$\Sigma F_Y=0 \rightarrow Y-F_{Y1}+F_{Y2}=0 \rightarrow Y=F_{Y2}-F_{Y1}$$

$$\Sigma F_Z=0 \rightarrow Z+F_{Z1}+F_{Z2}+F_{Z3}=0 \rightarrow Z=-F_{Z1}-F_{Z2}-F_{Z3}$$

$$\Sigma K_A=0 \rightarrow K=(F_{Y1}-F_{Y2})*Z_H+F_{Z1}-F_{Z2})*Y_{Z1}$$

$$\Sigma M_A=0 \rightarrow M=-F_{X1}*Z_H+(F_{Z1}+F_{Z2})*X_{Z2}-F_{Z3}*X_{Z3}$$

$$\Sigma N_A=0 \rightarrow N=(F_{Y2}+F_{Y1})*X_{Y2} \qquad (21)$$

Design of Experiments

The following considerations were taken in the process of designing these experiments:

- All experiments needed to be conducted at a constant velocity. The goal of these experiments was to measure steady forces (only dependent on the steady velocity of the vessel). Added mass (resulting from acceleration) and hydrostatic forces were studied separately with different approach. The experiments were designed to be done at 6 values of velocities: 0.25, 0.5, 1, 1.5, 2 and 2.5 m/s.

- As the rudder angle was one of the key factors in the maneuvering behavior of a vessel, the second parameter studied was rudder angle. 5 values of rudder angle were selected in the design: ±30, ±15 and 0 degrees.
- During maneuvers, the yaw angle of the vessel fluctuated which significantly affects the forces applied to the vessel. Hence, the third factor to be studied was the yaw angle. The yaw angles designed for the experiments were ±30, ±15 and 0 degrees.
- For each individual experiment, the model was fixed in all degrees of freedom excluding surge. This provides a steady range for each experiment to study forces applied to the vessel in each experimental setup.

Table 12 shows the experimental setup for all experiments:

Table 12- Experimental setup for towing experiments

Test #	Yaw Angle	Rudder Angle	Velocity (m/s)	Test #	Yaw Angle	Rudder Angle	Velocity (m/s)
1	0	0	0.5	31	15	15	1.5
2	0	0	1	32	15	15	2
3	0	0	1.5	33	-15	15	0.5
4	0	0	2	34	-15	15	1
5	30	0	0.5	35	-15	15	1.5
6	30	0	1	36	-15	15	2
7	30	0	1.5	37	-30	15	0.5
8	30	0	2	38	-30	15	1
9	15	0	0.5	39	-30	15	1.5
10	15	0	1	40	-30	15	2
11	15	0	1.5	41	0	30	0.5
12	15	0	2	42	0	30	1
13	-15	0	0.5	43	0	30	1.5

14	-15	0	1	44	0	30	2
15	-15	0	1.5	45	30	30	0.5
16	-15	0	2	46	30	30	1
17	-30	0	0.5	47	30	30	1.5
18	-30	0	1	48	30	30	2
19	-30	0	1.5	49	15	30	0.5
20	-30	0	2	50	15	30	1
21	0	15	0.5	51	15	30	1.5
22	0	15	1	52	15	30	2
23	0	15	1.5	53	-15	30	0.5
24	0	15	2	54	-15	30	1
25	30	15	0.5	55	-15	30	1.5
26	30	15	1	56	-15	30	2
27	30	15	1.5	57	-30	30	0.5
28	30	15	2	58	-30	30	1
29	15	15	0.5	59	-30	30	1.5
30	15	15	1	60	-30	30	2

A second series of experiments was designed and conducted afterward to achieve following goals: the first additional set of findings was used to study the effect of higher velocities on the forces, which enabled the development of a more comprehensive and accurate mathematical model. In the second series of additional experiments, 5 random experiments were selected to be conducted again to provide means of uncertainty analysis.

Table 13- - Experimental setup for additional towing experiments

Test #	Angle of Attack	Rudder Angle	Velocity (m/s)
61	0	30	2.5
62	0	15	2.5
63	0	0	2.5

19 re	-30	0	1.5
32 re	15	15	2
60 re	-30	30	2
17 re	-30	0	0.5
55 re	-15	30	1.5

5 Results and discussion

The final results of the experiments are the forces and moments transformed to the center of gravity in the body-fixed coordinate system at each experimental point. The following table presents the results:

Table 14- Summary of experimental results

Test #	Yaw Angle	Rudder Angle	Velocity (m/s)	Surge (N)	Sway (N)	Heave (N)	Roll (Nm)	Pitch (Nm)	Yaw (Nm)
1	0	0	0.5	3.53	2.31	1.30	-12.28	4.98	0.26
2	0	0	1	22.21	1.16	6.07	-33.31	54.91	0.28
3	0	0	1.5	47.97	-9.86	10.09	-37.63	139.99	-3.40
4	0	0	2	66.53	-12.22	30.23	-55.19	190.30	-7.52
5	30	0	0.5	7.65	-70.02	-7.80	192.39	131.65	-1.87
6	30	0	1	32.12	-295.31	-34.15	816.14	529.79	-10.24
7	30	0	1.5	61.15	-721.97	-88.31	2011.77	1277.36	-28.00
8	15	0	0.25	0.86	-10.35	-1.80	29.82	19.01	-0.18
9	15	0	0.5	1.41	-44.29	-8.28	127.15	73.75	-0.90
10	15	0	1	8.78	-195.62	-38.27	562.96	333.25	-6.94
11	15	0	1.5	17.70	-476.67	-101.48	1370.80	789.41	-22.65
12	15	0	2	35.12	-836.36	-170.66	2407.02	1392.66	-46.46
13	-15	0	0.25	1.24	11.20	3.49	-34.82	-16.34	0.31
14	-15	0	0.5	5.08	40.98	10.25	-127.26	-56.17	0.93
15	-15	0	1	23.21	181.70	44.56	-561.92	-241.98	6.40
16	-15	0	1.5	53.48	450.45	94.88	-1375.54	-589.64	21.51
17	-15	0	2	97.12	807.16	157.66	-2450.69	-1061.31	42.00
18	-30	0	0.25	3.71	18.22	3.54	-57.97	-21.46	0.62
19	-30	0	0.5	11.60	70.02	15.37	-219.39	-88.21	2.54
20	-30	0	1	49.66	287.79	67.65	-891.05	-353.45	10.37
21	-30	0	1.5	107.18	697.33	147.20	-2147.37	-872.11	29.99
22	0	15	0.25	0.74	0.01	-0.73	-1.95	1.24	0.01
23	0	15	0.5	3.68	3.55	1.06	-15.90	3.19	0.53
24	0	15	1	22.63	8.79	6.62	-56.67	43.47	1.64
25	0	15	1.5	49.53	10.17	13.17	-98.00	111.60	-0.93
26	0	15	2	69.03	14.74	37.44	-137.18	152.56	-3.43
27	30	15	0.25	2.20	-18.32	-2.91	50.86	34.74	-0.41

28	30	15	0.5	7.21	-67.85	-7.48	186.66	127.09	-1.51
29	30	15	1	26.74	-287.73	-29.87	798.32	514.21	-8.91
30	30	15	1.5	55.33	-709.19	-90.07	1985.28	1242.36	-25.91
31	15	15	0.25	0.67	-11.43	-2.59	33.21	20.06	-0.19
32	15	15	0.5	1.37	-42.93	-7.88	123.57	72.00	-0.72
33	15	15	1	8.45	-186.02	-37.45	536.39	319.04	-5.12
34	15	15	1.5	17.83	-466.87	-100.62	1343.17	777.02	-19.83
35	15	15	2	38.57	-805.54	-161.82	2315.49	1357.61	-38.70
36	-15	15	0.25	2.07	10.07	0.72	-31.88	-12.19	0.35
37	-15	15	0.5	5.55	43.62	8.60	-134.73	-59.33	1.48
38	-15	15	1	24.54	191.64	46.68	-592.43	-252.88	7.70
39	-15	15	1.5	58.31	465.34	95.09	-1423.16	-601.76	24.43
40	-15	15	2	104.68	848.13	158.53	-2578.23	-1103.58	50.63
41	-30	15	0.25	3.37	19.99	4.72	-62.05	-24.86	0.82
42	-30	15	0.5	13.91	70.77	16.77	-224.48	-83.51	3.08
43	-30	15	1	53.84	294.17	71.19	-913.01	-352.10	11.31
44	-30	15	1.5	110.88	713.06	149.89	-2197.86	-886.84	32.69
45	0	30	0.25	1.32	1.44	-0.16	-5.65	0.89	0.11
46	0	30	0.5	3.88	1.34	0.77	-9.41	6.80	0.43
47	0	30	1	24.28	9.84	6.50	-62.30	46.50	2.17
48	0	30	1.5	54.87	17.41	13.53	-127.13	115.90	1.95
49	0	30	2	78.02	26.13	36.31	-183.81	161.20	2.17
50	30	30	0.25	1.75	-20.51	-2.85	57.25	36.46	-0.49
51	30	30	0.5	7.47	-66.67	-7.05	182.37	126.26	-1.24
52	30	30	1	27.49	-282.05	-31.78	779.77	508.74	-6.88
53	30	30	1.5	58.65	-694.24	-89.37	1935.60	1230.41	-21.58
54	15	30	0.25	0.98	-11.01	-1.35	31.69	20.13	-0.13
55	15	30	0.5	1.70	-41.90	-7.01	120.33	71.22	-0.57
56	15	30	1	9.99	-182.55	-35.81	524.04	318.47	-3.99
57	15	30	1.5	21.86	-444.54	-97.05	1272.34	755.22	-15.86
58	15	30	2	44.66	-793.73	-158.91	2271.88	1354.27	-34.14
59	-15	30	0.25	0.92	11.42	2.33	-35.33	-16.74	0.41
60	-15	30	0.5	4.78	44.04	10.09	-136.35	-60.92	1.72
61	-15	30	1	26.39	195.80	47.82	-605.75	-254.09	8.81
62	-15	30	1.5	62.58	475.46	94.79	-1457.31	-607.64	26.21
63	-15	30	2	112.70	864.84	158.76	-2636.74	-1105.81	54.77
64	-30	30	0.25	3.45	20.68	4.28	-64.19	-25.62	0.91
65	-30	30	0.5	12.62	72.34	16.44	-227.39	-88.79	3.25
66	-30	30	1	53.84	299.60	70.83	-927.78	-359.17	12.49

67	-30	30	1.5	110.24	732.29	148.72	-2251.64	-915.84	35.00
68	0	30	2.5	102.54	43.37	80.12	-258.75	187.75	2.13
69	0	15	2.5	88.88	16.22	76.81	-160.66	191.63	-4.10
70	0	0	2.5	97.21	0.72	63.97	-98.37	213.28	-1.66
71 (13 re)	-15	0	0.25	1.14	10.44	2.04	-34.09	-12.28	0.43
72 (14 re)	-15	0	0.5	4.76	39.86	8.15	-129.91	-45.26	1.38
73(15 re)	-15	0	1	23.75	180.35	43.01	-586.17	-194.95	8.45
74 (21 re)	-30	0	1.5	106.89	712.30	147.49	-2317.10	-825.80	44.60
75 (62 re)	-15	30	1.5	64.11	467.53	91.64	-1508.70	-484.16	37.59
76 (35 re)	15	15	2	35.12	-807.81	-164.96	2270.12	1049.77	-58.49
77 (49 re)	0	30	2	79.31	39.01	-662.30	14.15	300.79	3.60
78 (18 re)	-30	0	0.25	3.00	20.15	3.78	-65.73	-24.07	1.25
79 (19 re)	-30	0	0.5	12.80	67.18	14.42	-225.67	-74.68	4.05

These results represent forces acting on and moments about the center of gravity of the vessel in calm water condition at constant velocity. In the mathematical model these forces are considered as total of steady forces at a given velocity, yaw angle and rudder angle. Acceleration dependent forces (added mass), hydrostatic forces, and restoring moments are calculated separately and summed to steady forces to give the total forces and moments on the model.

To be able to use the above experimental results in the simulation, a mathematical model which fits the result must be employed. In the following, the method used to build this model is described.

5.1 Non-dimensional analysis

The approach taken to find a descriptive mathematical model was to use dimensionless coefficients of forces and moments. For instance, the dimensionless coefficient of drag is $C_d=2F_d/\rho v^2 A$. As the density of the fluid and projected area are both constant, dividing

the drag force by square of velocity would return a coefficient of drag force which is a dimensionless value. Experiments are then divided into groups with the same rudder angle. Consequently for each group, a non-linear 2D curve is fitted to match the trend of the drag coefficients.

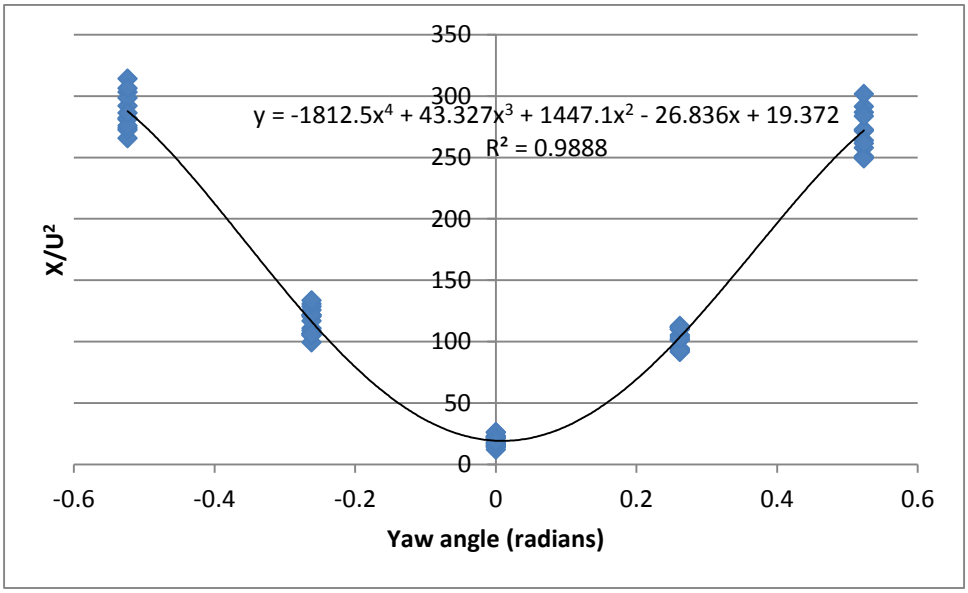

Figure 25- Surge coefficient vs yaw angle at effective rudder angle 0

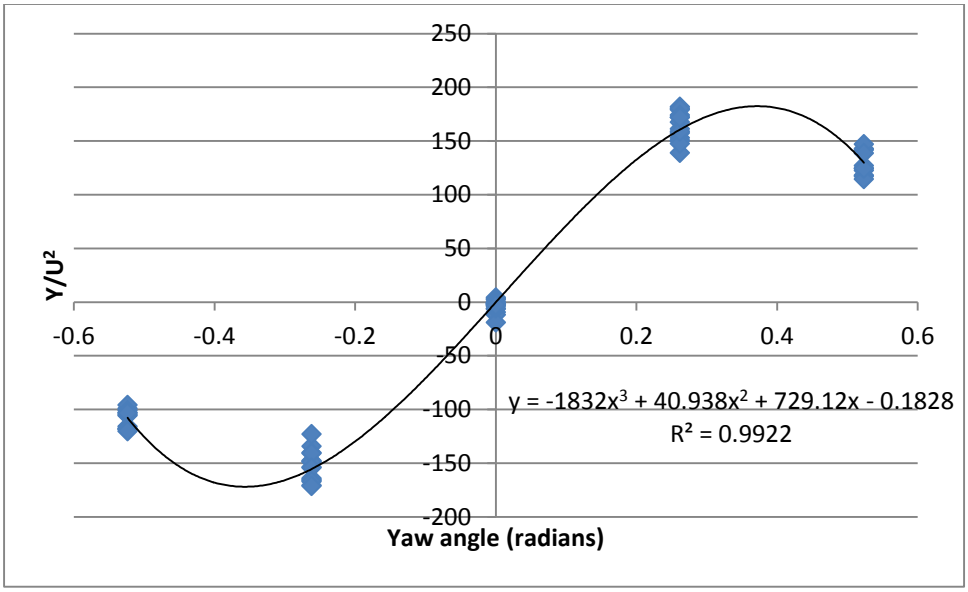

Figure 26- Sway coefficient vs yaw angle at effective rudder angle 0

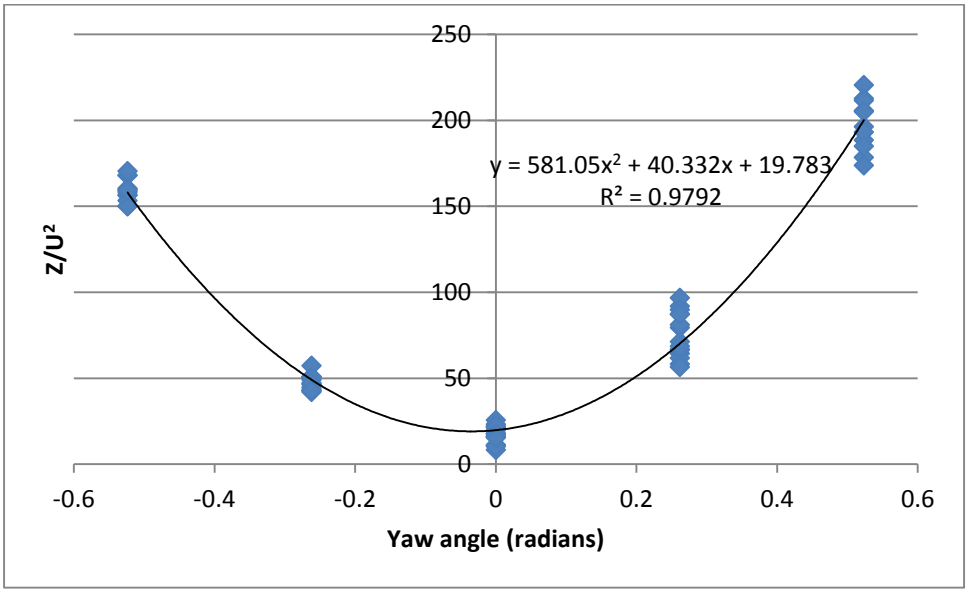

Figure 27- Heave coefficient vs yaw angle at effective rudder angle 0

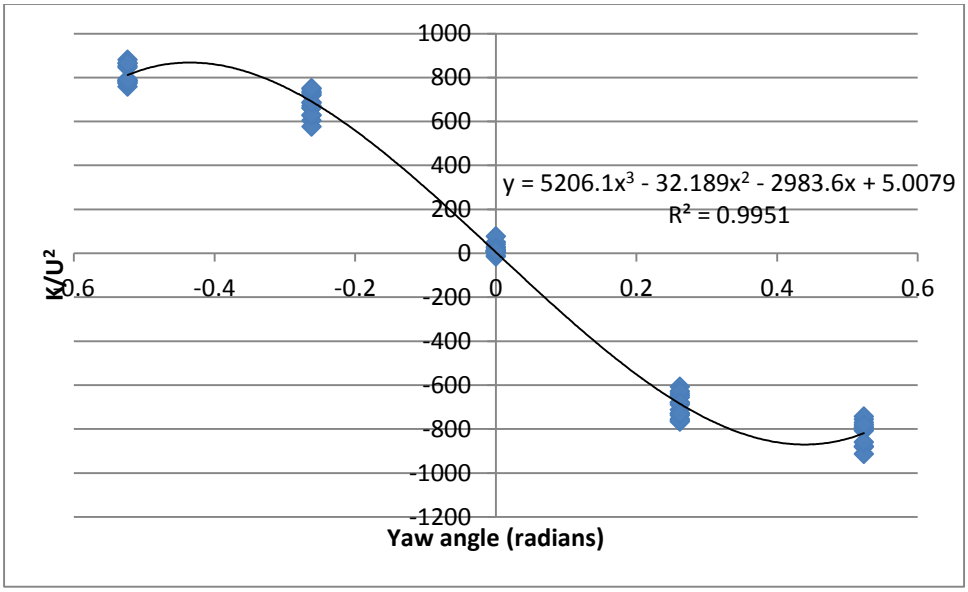

Figure 28- Roll coefficient vs yaw angle at effective rudder angle 0

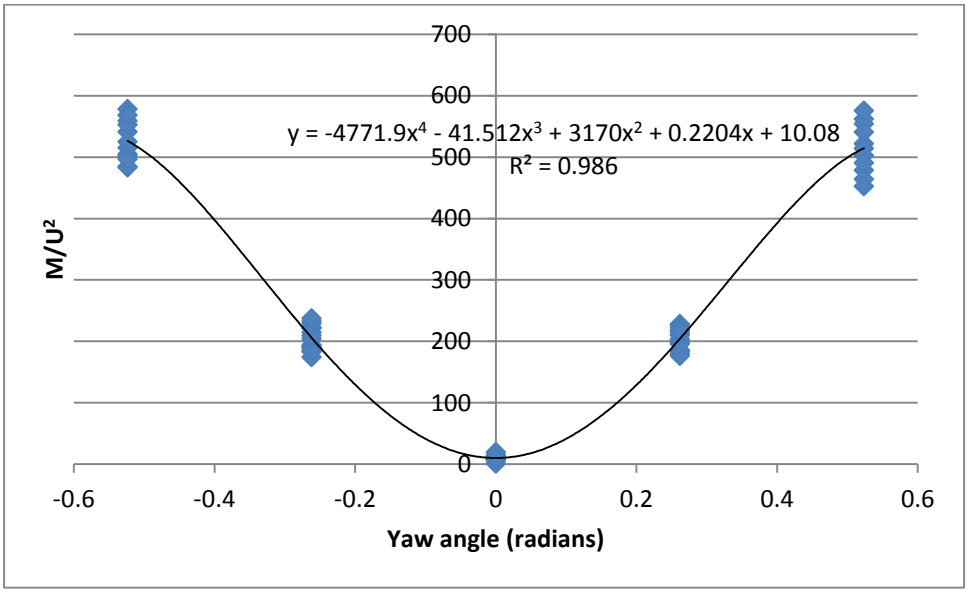

Figure 29- Pitch coefficient vs yaw angle at effective rudder angle 0

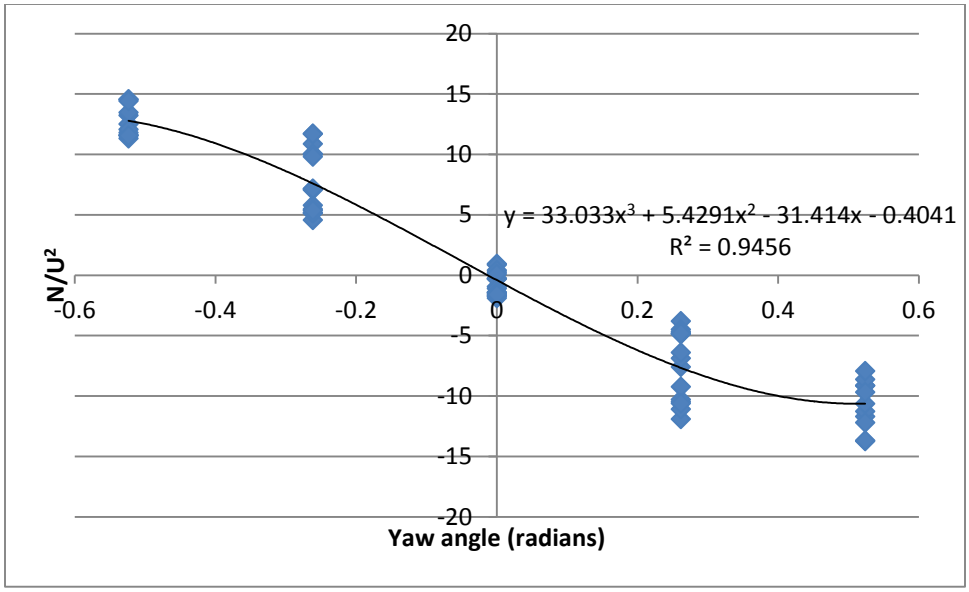

Figure 30- Yaw coefficient vs yaw angle at effective rudder angle 0

5.1.1 Scale effects

The complete hydrodynamic similarity between the model vessel and the full-scale vessel is not achievable in the reality (Bugalski et al. 2013). To achieve a valid model test, in which the hydrodynamic coefficients of maneuvering are same for the model and the full-scale, some hydrodynamic fluid parameter have to be satisfied. In particular, viscosity can affect the hydrodynamic forces of a maneuvering ship. It is impossible to satisfy this parameter during the model tests, the Reynolds number of the model test is to be equal to the Reynolds number of the full-scale ship that makes the hydrodynamic coefficient of the maneuvering of the model vessel not necessarily equal to the full-scale vessel.

In many cases, where the "scale effects" are estimated to be large, empirical formulations can be used to determine these scale effects (Abkowitz et al. 1988). For the case of this study, as the body geometry is not conventional, there is no available empirical

formulation to correct the hydrodynamic coefficients. For that, two possible solutions for the scaling effects could be suggested for further studies. First, CFD simulations for the both model-scale and full-scale vessel could achieve the hydrodynamic forces and coefficients of maneuvering in both scales and this can be used to study the scale effects. Second recommended procedure to determine the hydrodynamic coefficients for the full-scale vessel is to conduct some maneuvering experiments with the ship and use the system identification methods to estimate this coefficients (Bugalski et al. 2013). Both above mentioned solutions need considerable amount of time and resources and time and are beyond the scope of the project. So, for this study the scale effects are assumed to be negligible and not taken into consideration.

5.2 Simulation results

A mathematical model based on the equation of motion described in a previous chapter was developed to predict the trajectory of the propelled SPAR vessel in standard maneuvering trials. The Euler method to solve ordinary differential equations (ODEs) with time step 0.01 sec was employed for the simulations. The initial values of the total of forces, accelerations and velocities in all directions were zeros as all the simulation were started in steady state.

The standard 10˚/10˚ , 20˚/20˚ and 30˚/30˚ zig-zag maneuver (z-maneuver) and turning circle maneuver at 20˚ and 30˚ rudder were simulated. The simulation results are presented for the model size vessel.

Of particular interest, in these simulation results, is the extent of roll and pitch motions that are caused by the maneuvering forces. For conventional vessels, maneuvering models traditionally neglect the roll and pitch motions, but in the case of a propelled SPAR vessel, these motions are expected to be significant in magnitude and thus a significant factor in the vessel design. Thus the model developed here includes simulation of roll and pitch motions.

5.2.1 Turning circle maneuver

In a turning circle maneuver, after the vessel reaches a steady speed with zero yaw rate, the rudder angle is changed to a new setting and maintained for the rest of the experiment. The vessel response to this action is to turn in a circle. After reaching a steady state, the information to be obtained is:

- Tactical diameter
- Advance
- Transfer
- Loss of speed on steady turn
- Time to change heading 90 degrees
- Time to change heading 180 degrees

Figures 29-30 indicate the simulation results of the turning circle maneuver with the rudder angle of 20˚ and 30˚ for the model scale vessel L7.

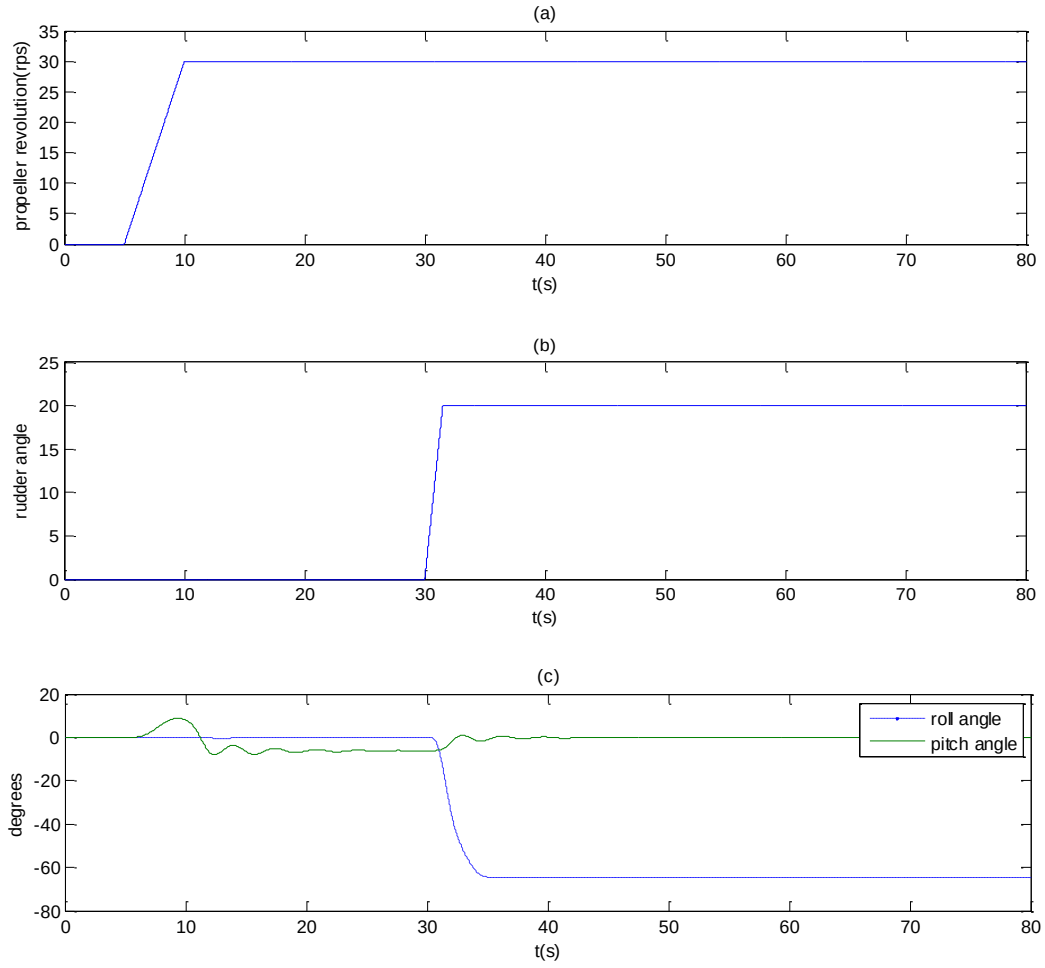

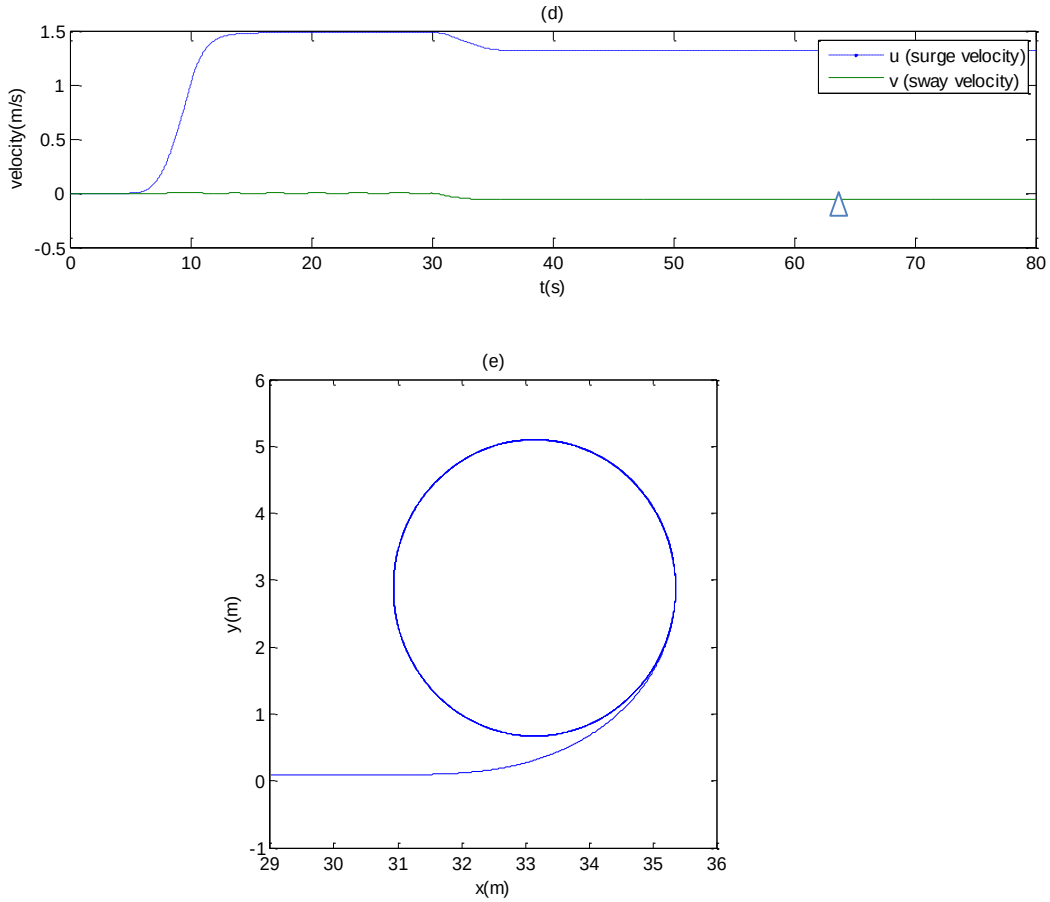

Figure 31- Simulation results of 20˚ turning circle maneuver for L7 model (a) propeller revolution vs time (b) rudder angle vs time (c) roll and pitch angle vs time (d) surge and sway velocity vs time (e) trajectory in earth-fixed coordinate system

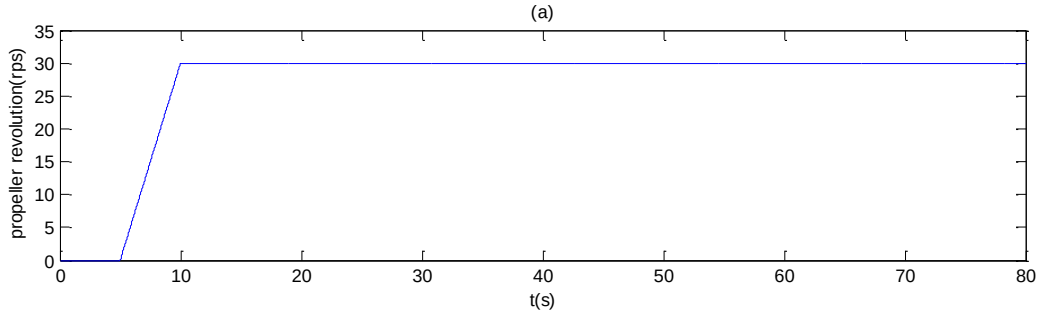

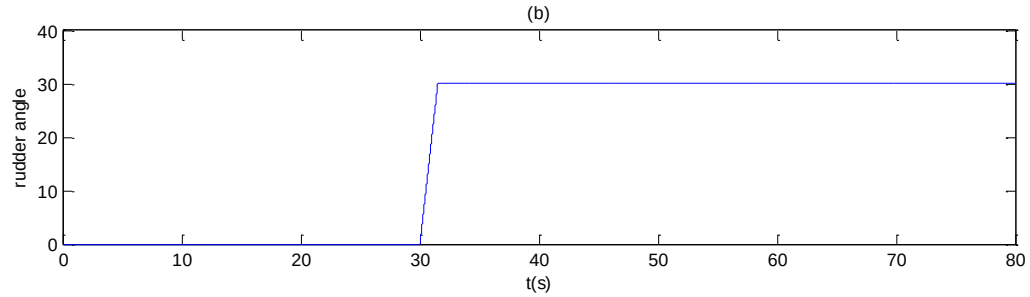
(b)
rudder angle
t(s)

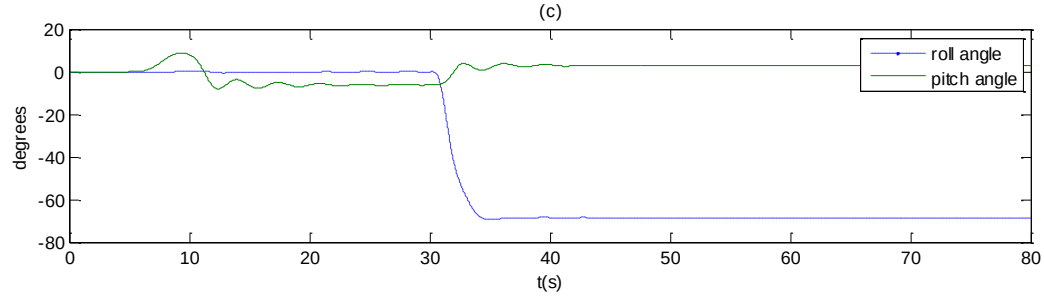
(c)
roll angle
pitch angle
degrees
t(s)

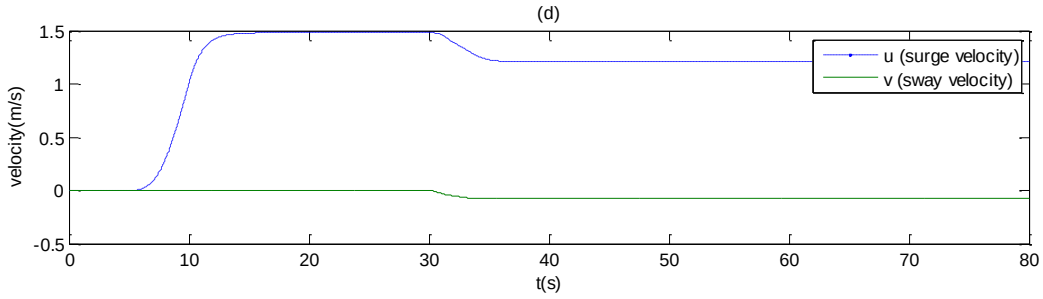
(d)
u (surge velocity)
v (sway velocity)
velocity(m/s)
t(s)

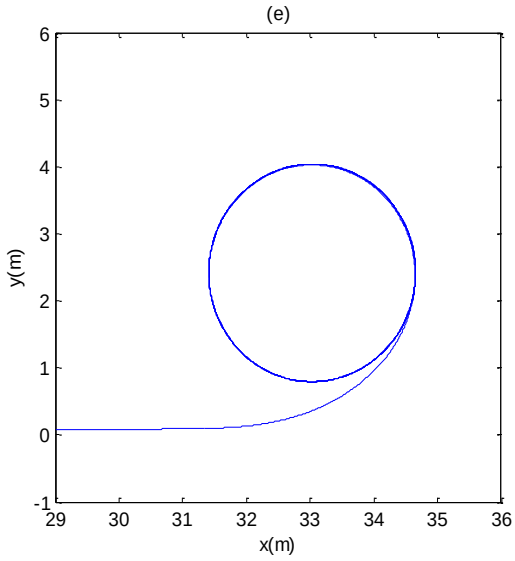
(e)
y(m)
x(m)

Figure 32- Simulation results of 30˚ turning circle maneuver for L7 model (a) propeller revolution vs time (b) rudder angle vs time (c) roll and pitch angle vs time (d) surge and sway velocity vs time (e) trajectory in earth-fixed coordinate system

The turning circle simulation shows relatively high maximum roll angles of 62˚ for the 20˚ turning circle maneuver and 67˚ for the 30˚ turning circle maneuver. The main reason for the high roll motion during maneuvers and high pitch motion during course changing is the high ratio of draft to length of the vessel. This characteristic motion might be partially reduced by lowering the center of gravity and consequently increasing the restoring forces.

Table 15 presents turning circle maneuvering parameters of the vessel in the simulation.

Table 15- Turning circle maneuvering parameters

	L7 δ=20˚	L1 δ=20˚	L7 δ=30˚	L1 δ=30˚
Tactical diameter	4.7	31	3.2	22.7
Advance	4.9	30.4	3.96	25.7
Transfer	5.05	34.5	4	27
Loss of speed on steady turn	0.16	0.4	0.25	0.65
Time to change heading 90 degrees	4.6	11.3	3.92	9.7
Time to change heading 180 degrees	7.3	18.6	6.1	15.4
Maximum roll angle (degrees)	9	62	9	62
Maximum pitch angle (degrees)	9	67	9	67

5.2.2 Zig-Zag maneuver

In a zig-zag maneuver, the rudder angle is reversed by δ degrees alternately to either side at a deviation Ψ from the initial course. After the vessel reaches a steady state, the rudder angle changes to δ and maintains this setting until the heading angle is Ψ degrees off the

initial course; then the rudder is reversed by the same angle. This procedure continues and results in a zig-zag trajectory for the vessel.

The most common values for the change of the heading angle are 10˚/10˚ and 20˚/20˚. The 30˚/30˚ zig-zag maneuver was also simulated for this study. The main results of the zig-zag maneuver follow (ITTC 2002b):

- Initial turning time (sec)
- Execute heading angle (degrees)
- Overshoot angle (degrees)
- Reach (sec)
- Time of a complete cycle (sec)
- Angular speed (deg/sec)

Figures 31-33 demonstrate the simulation results of the 10˚/10˚, 20˚/20˚ and 30˚/30˚ zig-zag maneuver for the model scale vessel L7 and Table 16 shows the zig-zag maneuvering parameters of the vessel in the simulation. The Δ sign in the x-y diagrams indicate the rudder activation point.

Table 16- Zig-zag maneuvering parameters

	L7 10˚/10˚	L1 10˚/10˚	L7 20˚/20˚	L1 20˚/20˚	L7 30˚/30˚	L1 30˚/30˚
Initial turning time (s)	3.7	9.4	4.1	10.8	4.7	11.7
Execute heading angle (degrees)	11.2	11	22.1	22	32.5	32.8

Overshoot angle (degrees)	2.65	1.25	4.5	4.45	4.17	5.9
Reach (sec)	9.1	20.1	9.4	25	12.8	26.5
Time of a complete cycle (sec)	17.6	39.2	18.4	48.7	25.2	52.3
Angular speed (deg/sec)	3.4	1.4	6	2.3	7.9	3

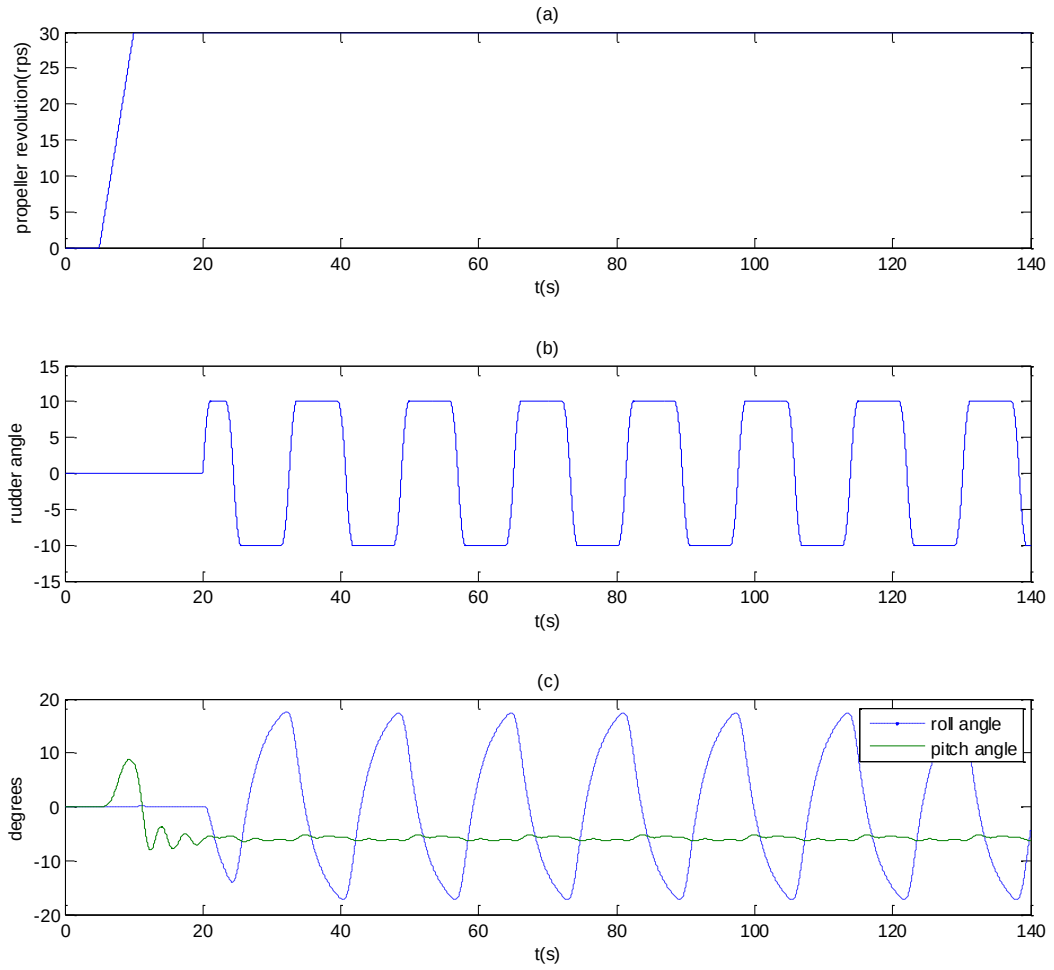

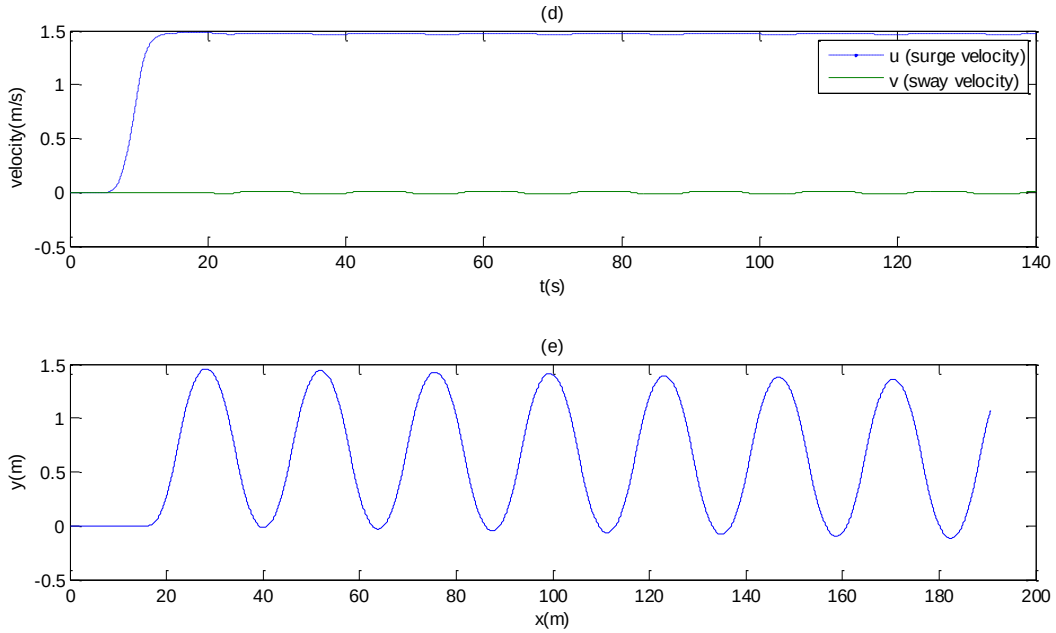

Figure 33- Simulation results of 10˚ zig-zag maneuver for L7 model (a) propeller revolution vs time (b) rudder angle vs time (c) roll and pitch angle vs time (d) surge and sway velocity vs time (e) trajectory in earth-fixed coordinate system

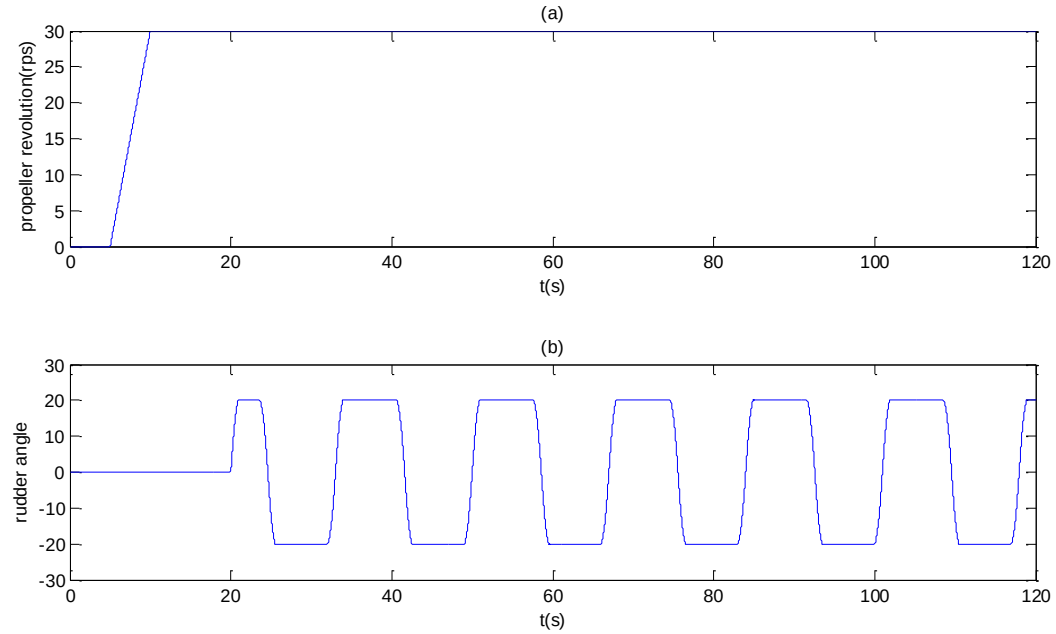

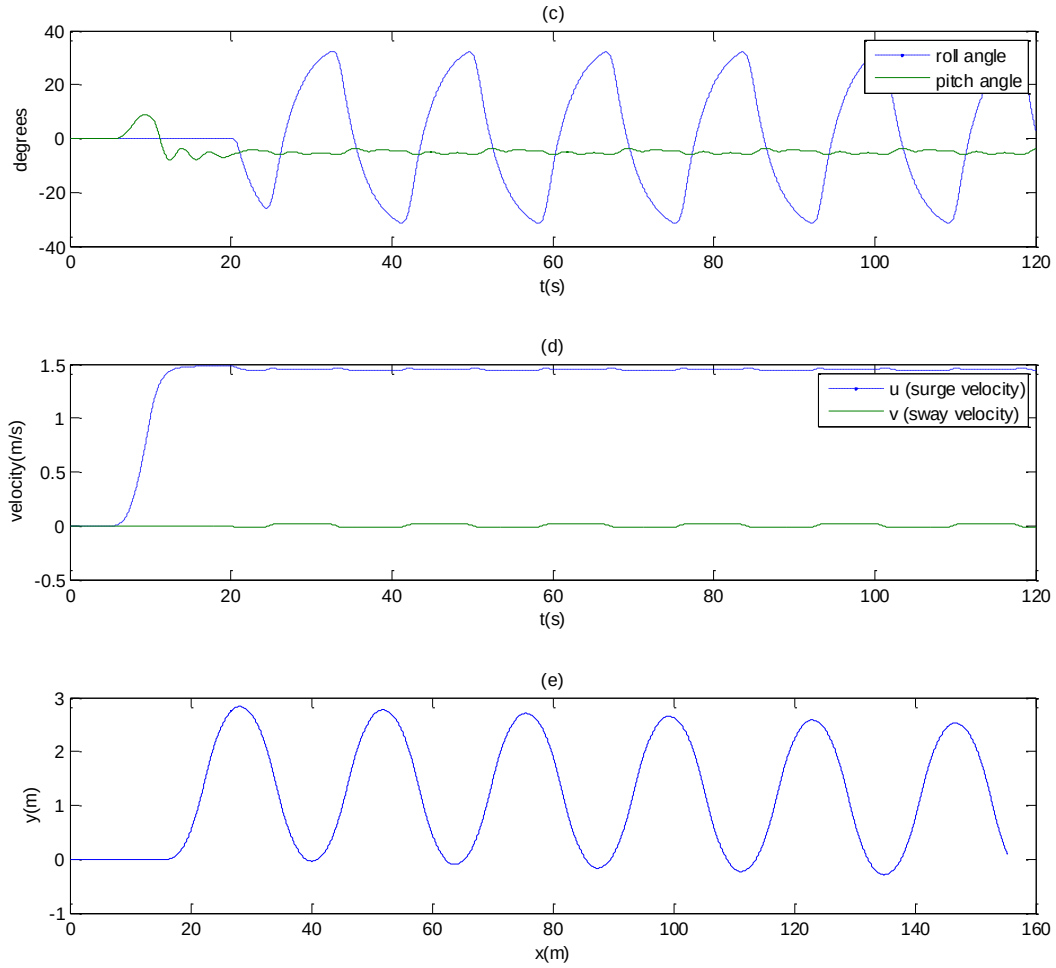

Figure 34- Simulation results of 20° zig-zag maneuver for L7 model (a) propeller revolution vs time (b) rudder angle vs time (c) roll and pitch angle vs time (d) surge and sway velocity vs time (e) trajectory in earth-fixed coordinate system

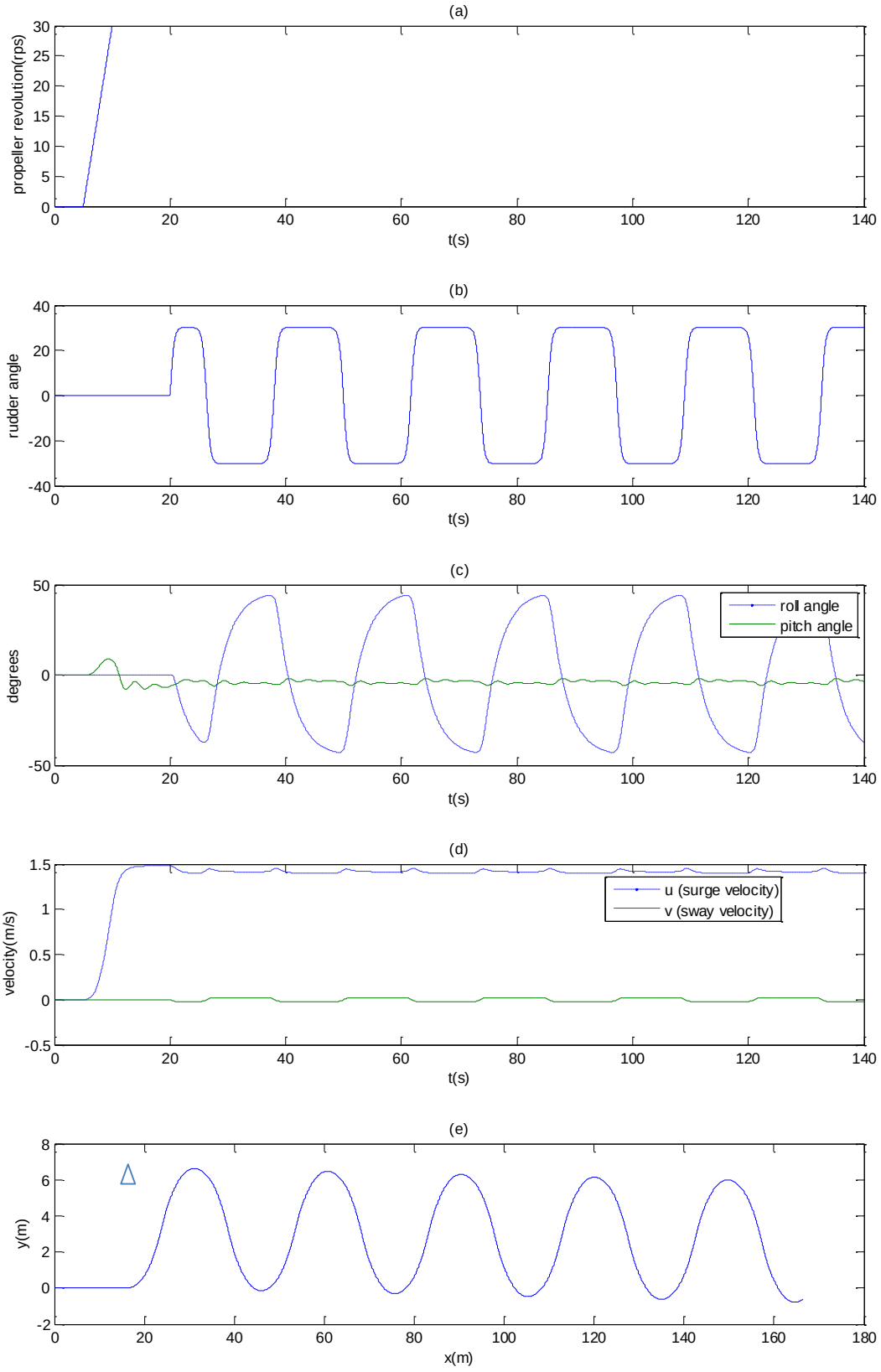
(a)
propeller revolution(rps)
t(s)
(b)
rudder angle
t(s)
(c)
degrees
roll angle
pitch angle
t(s)
(d)
velocity(m/s)
u (surge velocity)
v (sway velocity)
t(s)
(e)
y(m)
x(m)

Figure 35- Simulation results of 30˚ zig-zag maneuver for L7 model (a) propeller revolution vs time (b) rudder angle vs time (c) roll and pitch angle vs time (d) surge and sway velocity vs time (e) trajectory in earth-fixed coordinate system

The simulation results indicate that the maximum magnitude of the roll angle in the 20˚/20˚ zig-zag maneuvering is 27° and is around 48° for the 30˚/30˚ test. Moreover, changing the rudder angle from 20˚ to 30˚ doesn't significantly affect the performance of the vessel. This indicates a sharp increase in roll angle during the larger zig-zag turn.

It also must be considered that the most significant pitch moment of the vessel happens during acceleration, so steering and rolling motion do not play an important role in the pitch motion of the vessel.

6 Conclusion

In this study, a mathematical model for the maneuvering of the propelled SPAR was built and the hydrodynamic coefficients were determined by conducting captive model tests. The following can be concluded:

- The hydrodynamic forces on the hull, propeller and rudder were separately investigated and then combined in the mathematical model. The interactions between rudder and hull forces were taken into account as the rudder was installed during the captive model tests, so the measured forces were the result of hull and rudder forces and their interaction. The interaction between propeller thruster and hull was also estimated by the thrust deduction factor; however, the estimated amount of the thrust deduction factor was not validated. The interaction between propeller and rudder forces was not studied.
- The interactions between velocity and acceleration dependent components were neglected in the mathematical model (quasi steady approach). Although the hydrodynamic forces on a ship consist of complex combinations of steady and unsteady terms, it is assumed that neglecting the interactions between velocity and acceleration does not affect simulation results significantly.
- In the mathematical model developed for the propelled SPAR, the steady hydrodynamic forces were assumed to be functions of rudder angle, roll angle, angle of attack and surge velocity. Determining the effect of yaw rate on the

hydrodynamic forces by conducting planar motion tests might improve the accuracy of the prediction.

- The equations of motion used in this study consider the vessel as a rigid body with small pitch motions. The rigidity of the body is a safe assumption; the assumption of small magnitude of the pitch motion for this vessel type is acceptable only when the acceleration is not large, because the hydrodynamic derivatives of maneuvering are subject to change of high pitch angles.
- For simulating the maneuvering motion of a ship, the pitch and the roll motions are generally neglected. However, in this study the pitch and roll motions are incorporated, since previous free-running tests on the model showed significant rotational motion during the course-changing. These motions are clearly observed in the simulation results as well.
- The simulation result of the ship's motion in turning circle and zig-zag maneuvering shows high roll and high pitch motions during the course change. This characteristic is mainly the result of the long strut of the propelled SPAR. Simulation results state that the magnitude of these motions could be significantly diminished by lowering the center of gravity. For example by lowering the center of gravity by 10cm in the model, the magnitude of pitch motion is reduced by 50% and the magnitude of roll motion is reduced by 30% in the 20˚ turning circle test, and by 55% and 40% in the 20˚/20˚ zig-zag test respectively
- To validate the results of the simulations, a more controllable and instrumented vessel model is needed; however, the performance of the vessel is consistent with

the simulations and the motion properties of the vessel can be seen in the simulation.

- This maneuvering model is well developed and the predicted motions appear to be within a reasonable range based on limited experience with this vessel type. However the model needs to be validated (and possibly tuned) with full scale or model scale trials data for this vessel or a similar SPAR type vessel. Specially, it would be a useful next research step to test the SPAR model in a free-running configuration in the same standard maneuvers as were simulated.
- This numerical model (with some additional validation) can be used to optimize the design of a propelled SPAR type vessel particularly the aspect of limiting large amplitude pitch and roll motions or to establish operational guidelines to limit such motions during vessel maneuvers.

Bibliography

1. Abkowitz, M.A., 1964. *Lecture of Ship Hydrodynamics—Steering and Maneuverability, Hydro-and Aerodynamic Laboratory, Report No. Hy-5*,
2. Abkowitz, M.A., Member, L. & Liu, G., 1988. Measurement of Ship Resistance , Powering and Maneuvering Coefficients from Simple Trials During a Regular Voyage. *SNAME Transactions*, 96, pp.97–128.
3. Anon, 2015a. Penn Stainless Products. Available at: http://www.pennstainless.com/stainless-grades/precipitation-hardening/17-4-alloy-stainless-steel-2/ [Accessed November 3, 2015].
4. Anon, 2015b. *Wamit User Manual*, Chestnut Hill, MA. Available at: www.wamit.com.
5. Araki, M. Sadat-Hosseini, H., Sanada, Y., Tanimoto, K., Umeda, M., Stern, F., 2012. Estimating maneuvering coefficients using system identification methods with experimental, system-based, and CFD free-running trial data. *Ocean Engineering*, 51, pp.63–84. Available at: http://linkinghub.elsevier.com/retrieve/pii/S002980181200162X.
6. Bašić, J. & Parunov, J., 2013. Analytical and Numerical Computation of Added Mass in Ship Vibration Analysis. *Brodogradnja*, 64(2). Available at: http://hrcak.srce.hr/index.php?show=clanak&id_clanak_jezik=153618 [Accessed September 8, 2015].
7. Bernitsas, M.., Ray, D. & Kinley, P., 1981. *KT, KQ and Efficiency curvers for Wag b-series*, Michigan.
8. Blanke, M. & Knudsen, M., 1998. A sensitivity approach to identification of ship dynamics from sea trial data. *Proceedings of the IFAC Conference on Control Applications in Marine Systems (CAMS 1998)*, pp.261–270.
9. Bugalski, T., Streckwall, H. & Szantyr, J.A., 2013. Critical review of propeller performance scaling methods, based on model experiments and numerical calculations. *Polish Maritime Research*, 20(4), pp.71–79. Available at: http://www.degruyter.com/view/j/pomr.2013.20.issue-4/pomr-2013-0043/pomr-2013-0043.xml.
10. ExtremeOcean Innovation Inc., 2013. *Model Experiments of the ExtremeOcean ' s TranSPAR Craft*,
11. Fang, M., Luo, J. & Lee, M., 2005. A Nonlinear Mathematical Model for Ship

Turning Circle Simulation in Waves. *journal of ship research*, 49, pp.69–79.

12. Hirano, M., 1980. On Calculation Method of Ship Maneuvering Motion at Initial Design Phase. *Journal of the Society of Naval Architects of Japan*, 1980(147), pp.144–153. Available at: http://ci.nii.ac.jp/naid/110003878523/en/ [Accessed September 8, 2015].
13. ITTC, 2002a. *ITTC – Recommended Procedures*,
14. ITTC, 2002b. *ITTC – Recommended Procedures ITTC – Recommended Procedures Calibration of Steel Rulers*, http://ittc.info/. Available at: http://ittc.info/downloads/Archive of recommended procedures/2002 Recommended Procedures/7.5-04-02-01.pdf.
15. Lewandowski, edward m., 2004. *Dynamics of Marine Craft Maneuvering and Seakeeping.pdf*, Singapore: World Scientific Publishing Co. Pte. Ltd.
16. Luo, W., Moreira, L. & Guedes Soares, C., 2014. Manoeuvring simulation of catamaran by using implicit models based on support vector machines. *Ocean Engineering*, 82, pp.150–159. Available at: http://dx.doi.org/10.1016/j.oceaneng.2014.03.008.
17. Macneill, J.A., 2011. *THE DESIGN, MANUFACTURE & TESTING OF A PODDED PROPULSOR INSTRUMENTATION PACKAGE*. Memorial University of Newfoundland May.
18. Maimun, A., Priyanto, A., Muhammad, A. H., Scully, C. C., Awal, Z. I., 2011. Manoeuvring prediction of pusher barge in deep and shallow water. *Ocean Engineering*, 38(11-12), pp.1291–1299. Available at: http://dx.doi.org/10.1016/j.oceaneng.2011.05.011.
19. Millan, D. & Thorburn, P., 2009. *A Planar Motion Mechanism (PMM) for Ocean Engineering Studies*,
20. National Instruments, 2015. What Is Data Acquisition? - National Instruments. Available at: http://www.ni.com/data-acquisition/what-is/ [Accessed November 3, 2015].
21. Newman, J.N., 1977. *Marine Hydrodynamics*, London, England: MIT Press. Available at: https://books.google.ca/books/about/Marine_Hydrodynamics.html?id=nj-k_lAmaBYC&pgis=1 [Accessed September 8, 2015].
22. Orfano, F., 2009. Measuring hydrodynamic forces and moments on a ship with Rotating Arm Facility. Available at: http://www.brighthubengineering.com/marine-engines-machinery/23759-rotating-arm-facility-a-ship-motion-test/ [Accessed October 29, 2015].
23. Perez, T. & Blanke, M., 2002. *Mathematical Ship Modeling for Control*, Newcastle. Available at: http://www.iau.dtu.dk/secretary/pdf/TP-MB-shipmod.pdf.

24. Ross, A.,.T., Perez, and T., F., 2007. A novel maneuvering model based on low-aspect-ratio lift theory and lagrangian mechanics. In *Proceedings of the IFAC Conference on Control Applications in Marine System (CAMS).*

25. Toxopeus, S.L., 2009. Deriving mathematical manoeuvring models for bare ship hulls using viscous flow calculations. *Journal of Marine Science and Technology*, 14(1), pp.30–38.

26. Tran Khanh, T. et al., 2013. Assessment of ship manoeuvrability by using a coupling between a nonlinear transient manoeuvring model and mathematical programming techniques. *Journal of Hydrodynamics*, 25(5), pp.788–804. Available at: http://dx.doi.org/10.1016/S1001-6058(13)60426-6.

27. Yasukawa, H. & Yoshimura, Y., 2014. Introduction of MMG standard method for ship maneuvering predictions. *Journal of Marine Science and Technology*, 20(1), pp.37–52. Available at: http://link.springer.com/10.1007/s00773-014-0293-y.

28. Yoon, H.K. & Rhee, K.P., 2003. Identification of hydrodynamic coefficients in ship maneuvering equations of motion by Estimation-Before-Modeling technique. *Ocean Engineering*, 30(18), pp.2379–2404.

29. Yoshimura, Y., 2005. *Mathematical Model for Manoeuvring Ship Motion (MMG Model)*, Hokkaido.

30. Zaojian, Z., 2006. *SHIP MANOEUVRING AND SEAKEEPING*, Available at: http://naoce.sjtu.edu.cn/pna.

31. Zhang, X.G. & Zou, Z.J., 2011. Identification of Abkowitz model for ship manoeuvring motion using ε-support vector regression. *Journal of Hydrodynamics*, 23(3), pp.353–360. Available at: http://dx.doi.org/10.1016/S1001-6058(10)60123-0.

Appendix A – Load cells calibration and validation data

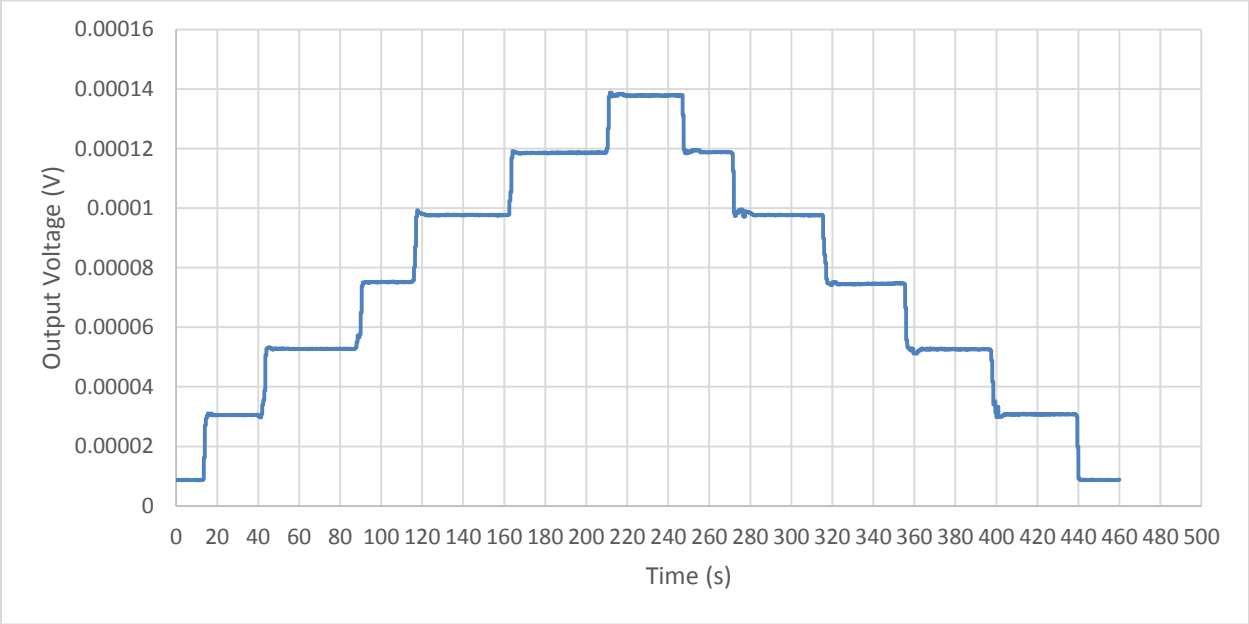

Figure 36- Load cell Y2 time series plot

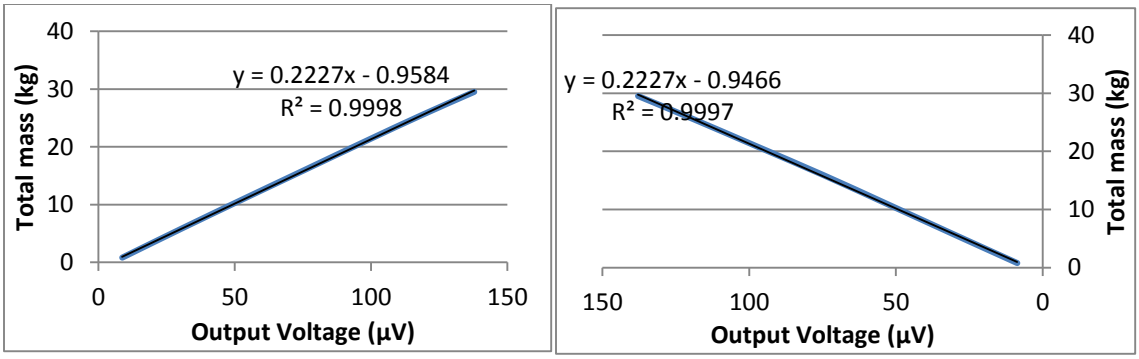

Figure 37- Calibration plot for loading (left) and unloading (right) load cell Y2

Table 17- Verification result for calibration of load cell Y2

Weight(g)	Voltage(V)	Prediction(g)	Error (%)
10864	5.30E-05	10846.1	-0.165
20931	9.81E-05	20906.1	-0.119

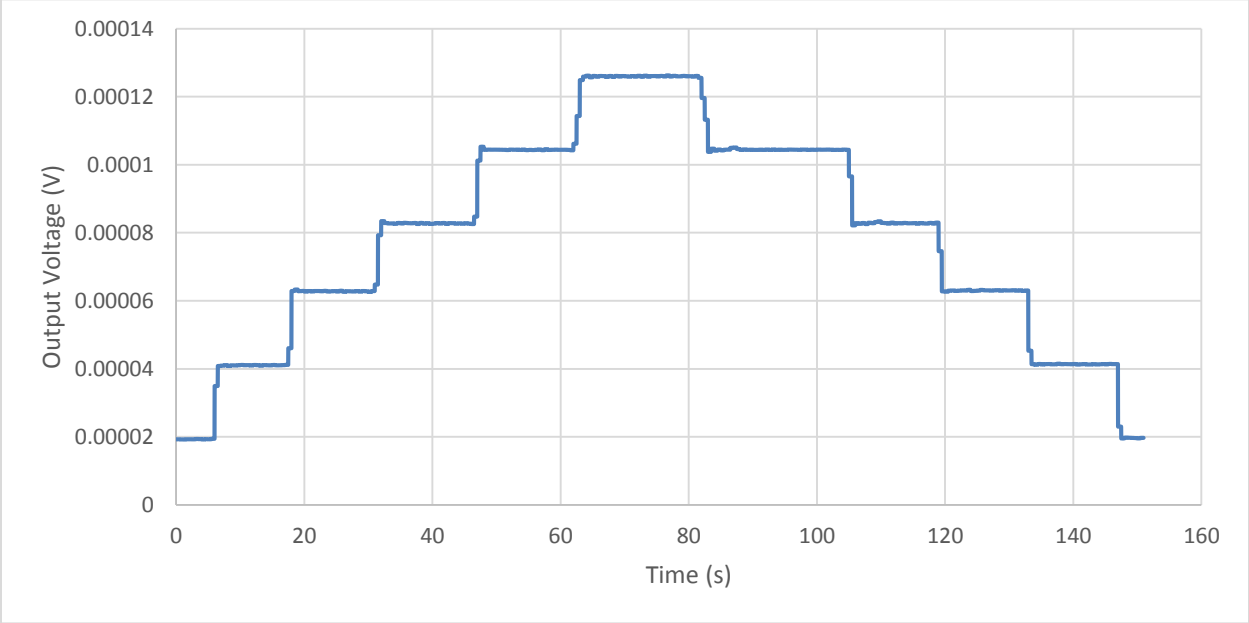

Figure 38-Load cell Z1 time series plot

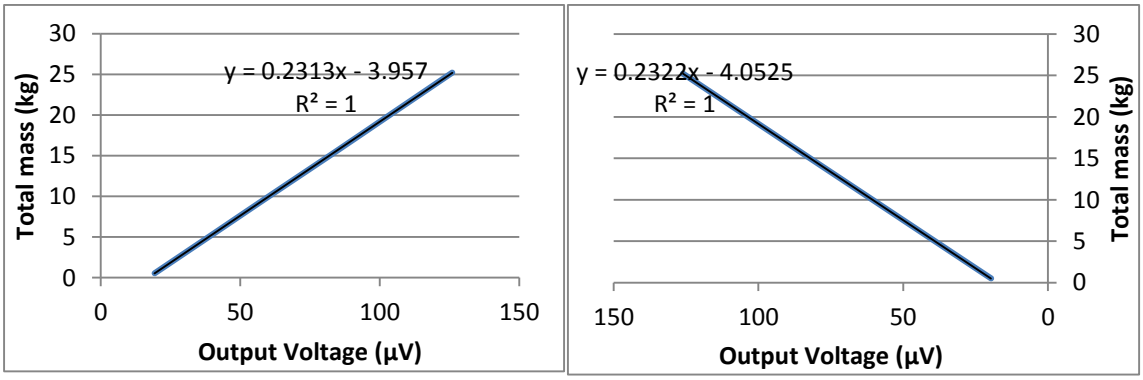

Figure 39- Calibration plot for loading (left) and unloading (right) load cell Z1

Table 18- Verification result for calibration of load cell Z1

Weight(g)	Voltage(V)	Prediction(g)	Error (%)
10613	6.31E-05	10622.3	-0.088
21031	1.08E-04	20867.7	-0.780

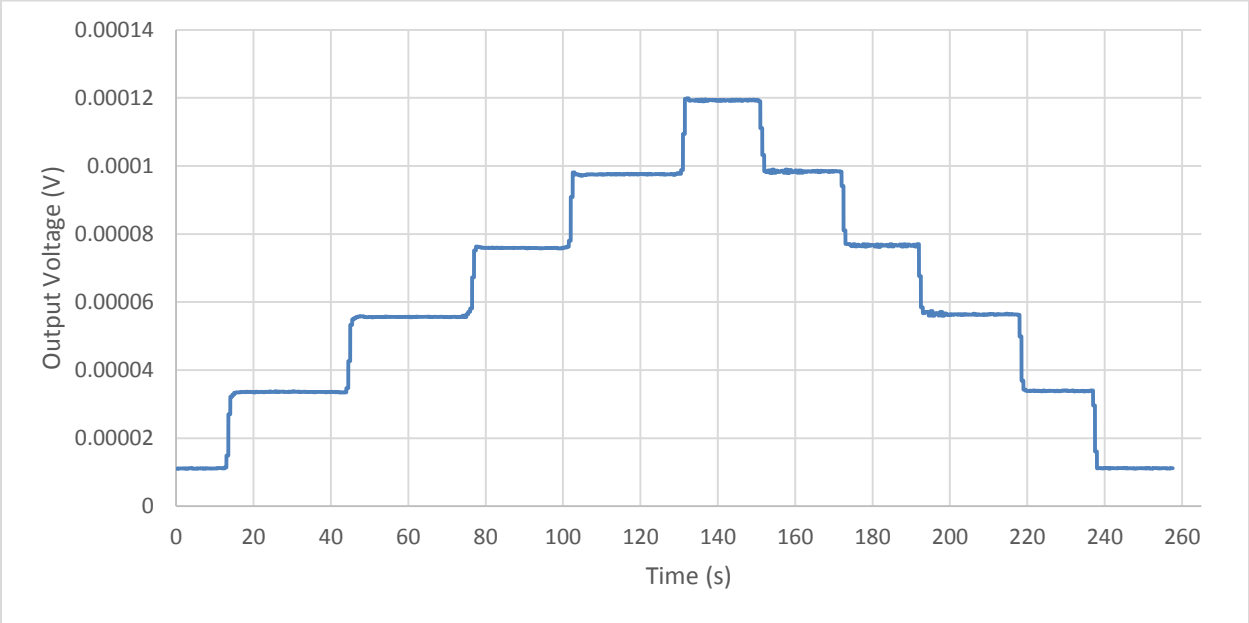

Figure 40- Load cell Z2 time series plot

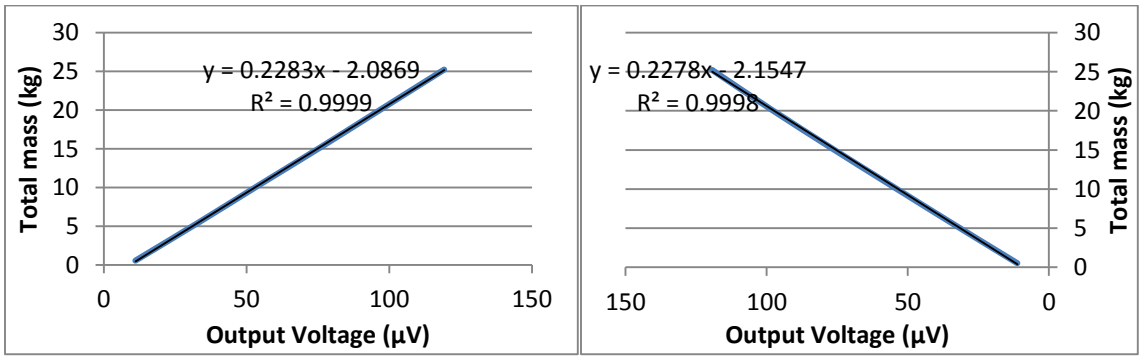

Figure 41- Calibration plot for loading (left) and unloading (right) load cell Z2

Table 19- Verification result for calibration of load cell Z2

Weight(g)	Voltage(V)	Prediction(g)	Error (%)
10613	5.54E-05	10511.4	0.957

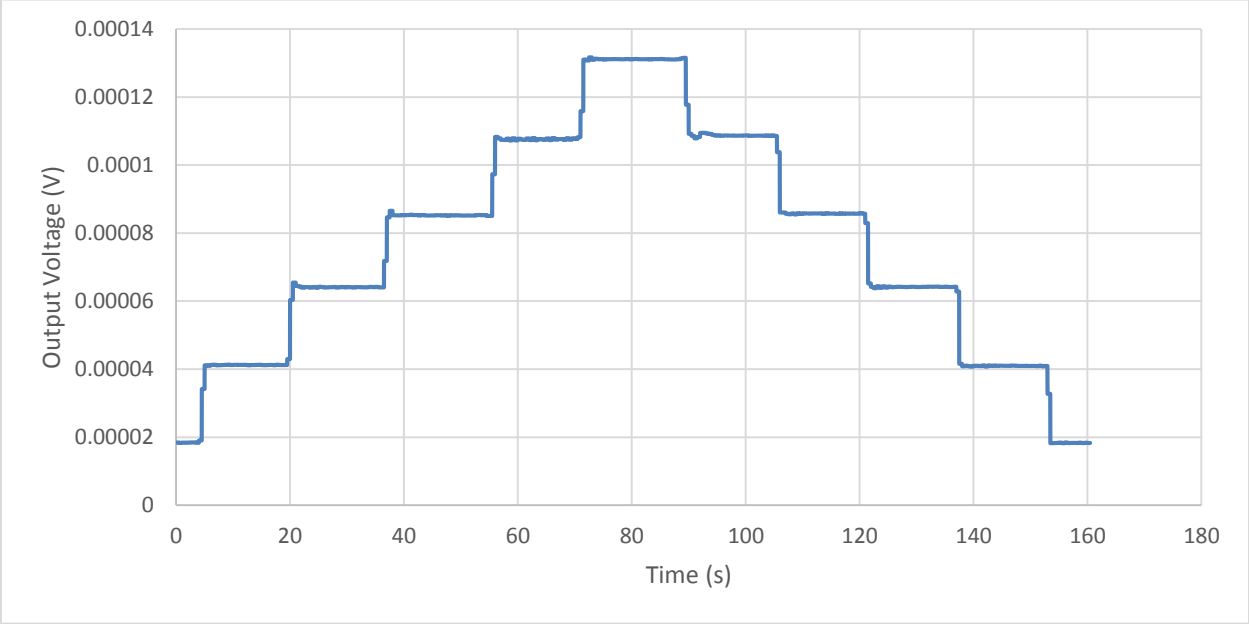

Figure 42- Load cell Z3 time series plot

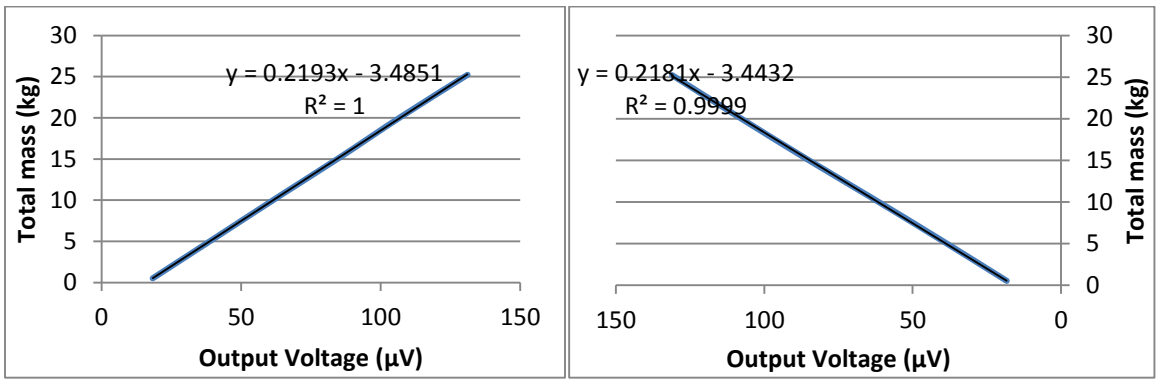

Figure 43- Calibration plot for loading (left) and unloading (right) load cell Z3

Table 20- Verification result for calibration of load cell Z3

Weight(g)	Voltage(V)	Prediction(g)	Error (%)
10613	6.45E-05	10607.3	0.054

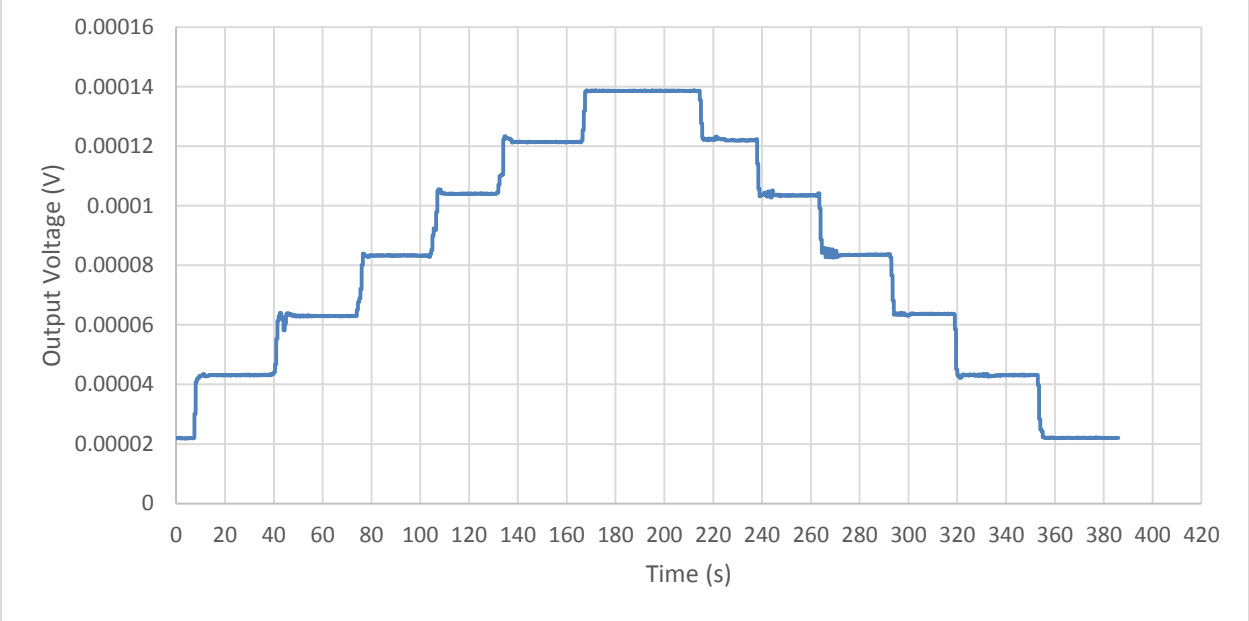

Figure 44- Load cell X1 time series plot

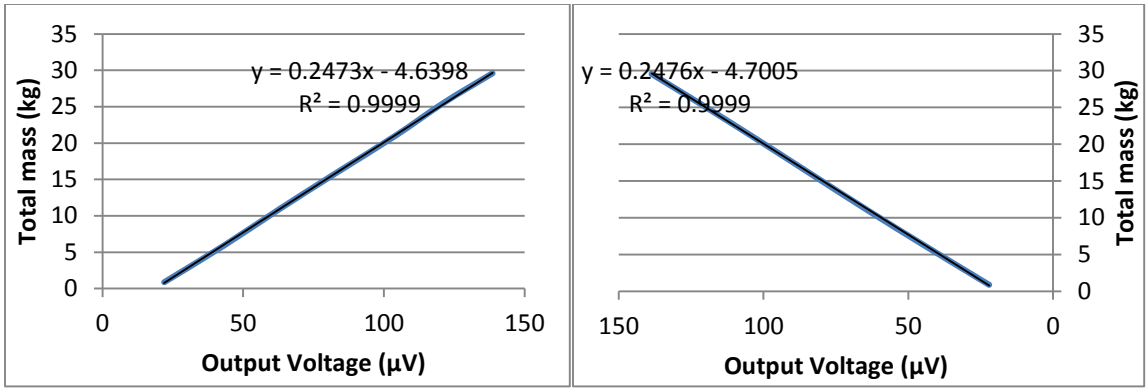

Figure 45- Calibration plot for loading (left) and unloading (right) load cell X1

Table 21- Verification result for calibration of load cell X1

Weight(g)	Voltage(V)	Prediction(g)	Error (%)
10922	6.34E-05	11025.5	0.948
20989	1.03E-04	20837.6	0.721